Order Number 9510721

Anisotropic ion temperature gradient instabilities

Song, Hao, Ph.D.

City University of New York, 1994

U·M·I
300 N. Zeeb Rd.
Ann Arbor, MI 48106

Anisotropic Ion Temperature Gradient Instabilities

by

HAO SONG

A dissertation submitted to the Graduate Faculty in Physics in partial fulfillment of the degree of Doctor of Philosophy, The City University of New York

1994

This manuscript has been read and accepted for the Graduate Faculty in Physics in satisfaction of the dissertation requirement for the degree of Doctor of Philosophy.

9/23/94
Date

Prof. Mark Hillery
Chair of Examining Committee

September 23, 1994
Date

Prof. Edward Tryon
Executive Officer

Prof. Ying Chen

Prof. Lawrence A. Ferrari

Prof. Arnold Kritz

Prof. John A. Krommes

Prof. Amiya K. Sen
Supervisory Committee

THE CITY UNIVERSITY OF NEW YORK

ABSTRACT

ANISOTROPIC ION TEMPERATURE GRADIENT INSTABILITIES

by

Hao Song

Advisor: Professor Amiya K. Sen

The effects of anisotropic temperature gradient and collisions on the ion-temperature-gradient (ITG) instabilities have been investigated by using kinetic theory. In the slab limit, the ITG mode is driven unstable by coupling between the transit resonance and ion temperature gradients. While $\eta_{i\perp}$ ($\eta_{i\perp} \equiv \partial \ln T_{i\perp}/\partial \ln n$, where $T_{i\perp}$ is the perpendicular ion temperature and n is the plasma density) only affects the mode through the finite Larmor radius effect, $\eta_{i\parallel}$ ($\eta_{i\parallel} \equiv \partial \ln T_{i\parallel}/\partial \ln n$) is needed to trigger the instability. With electron collisions, the mode propagating in the electron diamagnetic drift direction becomes more unstable at small $\eta_{i\perp}$ but a second stability regime is found at large $\eta_{i\perp}$ for the branch propagating in the ion diamagnetic drift direction. In the toroidal limit, the ion branch is driven unstable by coupling between the magnetic drift resonance and temperature gradients and it can be stabilized by electron collisions. The

electron branch destabilized by the interchange effect from bad magnetic curvature can be further destabilized by electron collisions. For the trapped ion toroidal ITG mode, the perpendicular ion temperature gradient is crucial to drive the instability. However, the critical temperature gradient is increased by a factor of $1/\varepsilon^{1/2}$, where $\varepsilon^{1/2}$ is the trapped fraction, and it can be further enlarged by ion or electron collisions. For the mixed slab and toroidal ITG mode, a coupling between the ion and electron branches was found to cause the stability regime to break into two separated regions in the $\eta_{i\parallel}$-$\eta_{i\perp}$ plane. Electron collisions can significantly reduce the first stability regime at small $\eta_{i\perp}$ but expand the second stability regimes at large $\eta_{i\perp}$. The non-local correction has a stabilizing effect on the ion branch but a destabilizing effect on the electron branch. This effect is so strong that it can overcome the coupling effect and so the second stability regime is not separated from the first one. The new second stability regime may provide a possible stabilization scheme for the ITG instability via intense ion cyclotron resonance heating and neutral beam injection.

ACKNOWLEDGEMENT

I wish to express my sincere gratitude to my advisor, Prof. Amiya Sen of Columbia University, for his insight, suggestion, and support, without which this thesis would not have been possible.

Also, my thanks go to Prof. Arnold Kritz of Lehigh University and Prof. John Krommes of Princeton University for their fruitful discussions. I am grateful to Dr. Rod Greaves and Dr. Bin Song as well as my fellow graduate students Jiong Chen, Philip Tham and Aki Sekiguchi for their friendship and assistance during all these years.

Finally, I wish to thank my wife, Lijun, for her forbearance and encouragement, and my newborn son, Rainbow, for providing a strong motivation to keep going on.

This thesis is dedicated to my mother.

This research was supported by U.S. Department of Energy Grant No. DE-FG02-87ER53257.

To the memory of my father, Zhongmo Song

CONTENTS

CHAPTER 1

INTRODUCTION

1.1. Previous work

The ion temperature gradient driven (ITG) instability was first formulated three decades ago (RUDAKOV *et al.*, 1961). It was found that with a flat density profile a mode could be driven unstable by an ion temperature gradient. The mode was essentially an electrostatic mode that propagates in the ion diamagnetic drift direction. The instability can be characterized by a critical parameter $\eta_i \equiv \partial \ln T_i / \partial \ln n$, where T_i is the ion temperature and n is the plasma density. Early analyses of the ITG instability were performed in the slab limit, with emphasis on the dynamics along the magnetic field **B**. Using the fluid-ion approximation, Coppi *et al.* (COPPI *et al.*, 1967) derived a mode equation, from which the threshold value of η_i was obtained. Kadomtsev *et al.* (KADOMTSEV *et al.*, 1970) suggested that the kinetic-ion effect should be taken into account and obtained a lower threshold $\eta_i \sim 1$. This was confirmed in detailed numerical studies by Waltz *et al.* (WALTZ *et al.*, 1980). Later, it was found (COPPI *et al.*, 1977, HORTON *et al.*, 1981) that the η_i mode can also be unstable in the toroidal limit. From fluid theory, Horton *et al.* (HORTON *et al.*, 1981) pointed out that the mode balloons significantly in the bad curvature region and is driven unstable by interchange effects. The kinetic effect on this mode has also been studied intensely. (TERRY *et al.*, 1982, GUZDAR *et al.*, 1983) Other relevant studies during that time

investigated particle and heat transport, (ANTONSEN *et al.*, 1979, HORTON *et al.*, 1980) quasi-linear (MIGLIUOLO, 1985) and nonlinear (LEE *et al.*, 1986) saturation mechanism.

Recently, ITG instability has received intense interest since it was suggested by many authors (TANG *et al.*, 1986, BIGLARI *et al.*, 1989, ROMANELLI *et al.*, 1989) that the ITG instability may be responsible for the anomalous heat transport in tokamaks. Supporting experimental evidence from many tokamak devices included the improvement in confinement time under more peaked density profile (GREENWALD *et al.*, 1984, KAUFMANN *et al.*, 1988, SCHISSEL *et al.*, 1989, JET Team *et al.*, 1989, SUZUKI *et al.*, 1989, SOLDNER *et al.*, 1988, WATARI *et al.*, 1990), a density fluctuation propagating in the ion diamagnetic direction (WATTERSON *et al.*, 1985), and strong anomalous heat transport with relatively flat density profiles (WANGER *et al.*, 1982, NAGAMI *et al.*, 1984, KAYE *et al.*, 1985). However, a more recent experiment (ZARNSTORFF *et al.*, 1991) performed on the tokamak fusion test reactor (TFTR) indicated that the threshold value of the ion temperature gradient was higher than the theoretical predictions from slab or toroidal ITG models (Tang *et al.*, 1986; BIGLARI *et al.*, 1989; ROMANELLI *et al.*, 1989; GUZDAR *et al.*, 1983). As the density profiles were broadened significantly, the ion thermal transport remained unchanged. To address this issue, more complex numerical studies of the η_i mode were undertaken. Xu and Rosenbluth (XU *et al.*, 1991) used a particle simulation code to study the ITG mode in a toroidal geometry with trapped ions. Dong *et al.* (DONG *et al.*, 1992) developed a kinetic integral equation for the study of the ITG instability in toroidal geometry. Kim *et al.* (KIM *et al.*, 1993) considered in detail the electron-magnetic effect on the toroidal ITG mode.

Moreover, present day tokamaks such as TFTR can approach such low collisionalities (ZARNSTORFF *et al.*, 1989) that both electrons and ions are in the 'banana regime' ($\nu_{*j} \equiv \nu_{eff,j}/\omega_{bj} < 1$, where $\nu_{eff,j}$ is the effective collision frequency and ω_{bj} the trapped particle bounce frequency of the *j*th species). Here, the particles with low parallel velocities are trapped in the outer part of the torus in a toroidal system. Although the collisionalities are low, the dissipative trapped electrons can still play an important role because the effective collision frequency can be much higher than the mode frequency. The trapped particle response can modify the results of the ITG mode. Romanelli *et al.* (ROMANELLI *et al.*, 1990) investigated the effect of trapped electrons on the toroidal η_i mode and found that the threshold value of the ion temperature gradient for the mode propagating in the electron diamagnetic drift direction can be removed by the destabilizing effect of the trapped electron response, while the threshold for the mode propagating in the ion diamagnetic drift direction persists.

1.2. Motivation of the present research

However, most of the theoretical studies on the η_i mode have omitted the possible different roles of the gradient of the parallel and perpendicular ion temperatures, henceforth denoted as $\eta_{i\parallel} \equiv \partial \ln T_{i\parallel}/\partial \ln n$ and $\eta_{i\perp} \equiv \partial \ln T_{i\perp}/\partial \ln n$, respectively. Because anisotropic ion temperature and the corresponding anisotropic ion temperature gradients can be generated by powerful auxiliary heating schemes such as ion cyclotron resonance heating (ICRH) and neutral beam injection (NBI), it is important to consider the effects of anisotropy in the ion temperature gradient (MATHEY *et al.*, 1989, KIM *et al.*, 1991). There are two important reasons of the further study. First, the investigation of the

different roles of parallel and perpendicular ion temperature gradients (i.e. $\eta_{i\parallel}$ and $\eta_{i\perp}$) furthers our understanding of the physics of the ITG instability. Secondly, only after this understanding can one address the important practical question of which heating methods should be used to produce more η_i stable plasma.

This effect was investigated first in the shearless slab geometry. Using a local kinetic theory, Mathey and Sen (MATHEY *et al.*, 1989) showed that a gradient in the parallel ion temperature is needed to excite the slab ITG instability, while a gradient in the perpendicular temperature can either enhance or reduce the instability. Kim *et al.* (KIM *et al.*, 1991) generalized the study to the toroidal limit by replacing the transit resonance with the magnetic drift resonance. They found that either a parallel temperature or perpendicular temperature gradient can have a destalibilizing effect.

In the present research, the model used by Mathey *et al.* (MATHEY *et al.*, 1989) is improved by including a realistic damping effect. This damping effect on the toroidal ITG mode discussed by Kim *et al.* (KIM *et al.*, 1991) is also examined. The study of the ITG mode is then extended to a circumstance where both the transit and the magnetic drift resonances are present. This allows us to study the more realistic situation in tokamaks, where mixed slab and toroidal ITG modes may be expected. Furthermore, the effect of trapped particles is included in the research. Unlike Romanelli *et al.* (ROMANELLI *et al.*, 1990), dissipative rather than semi-collisional trapped electrons are considered to focus on the effect of collisions. A simple model with trapped ions is used to explain the experimental results on TFTR (ZARNSTORFF *et al.*, 1991) and the Columbia Linear Machine (CLM) (GREAVES *et al.*, 1991). In addition, the non-local effect on the ITG mode is also included for completeness.

1.3. A fluid model of the η_i mode

A simple fluid model of the ITG instability is given in reference (TANG *et al.*, 1986). In the flat density gradient limit, the perturbed density response for the ions and electrons can be approximated by

$$n_i = n\frac{e\phi}{T_i}\left[-\frac{(1+\eta_i)\,\omega_{*i}\omega_{di}}{\omega^2} - \frac{k_\parallel^2 c_s^2 (1+\eta_i)\,\omega_{*i}}{2\omega^3}\left(\frac{T_i}{T_e}\right)\right]$$

and

$$n_e = n\frac{e\phi}{T_e}$$

where ω_{*i} is the ion diamagnetic drift frequency, and ω_{di} is the magnetic drift frequency. From the quasi-neutrality condition, the local dispersion relation is obtained as

$$1 + \frac{(1+\eta_i)\,\omega_{*i}\omega_{di}}{\omega^2}\left(\frac{T_e}{T_i}\right) + \frac{k_\parallel^2 c_s^2 (1+\eta_i)\,\omega_{*i}}{2\omega^3} = 0$$

Here, the second and third terms are the toroidal and slab contributions, respectively. In the slab limit ($\omega_{di} = 0$), the η_i instability is recovered, i.e.,

$$\omega = \left(\frac{-k_\parallel^2 c_s^2 (1+\eta_i)\,\omega_{*i}}{2}\right)^{1/3}\left(-\frac{1}{2} + i\frac{\sqrt{3}}{2}\right)$$

This result shows that the mode can be driven unstable by large η_i in the flat density gradient limit.

1.4. A kinetic model of the η_i mode

A kinetic model of the slab ITG instability can be found in reference

(MIKHAILOVSKII, 1974). Now, the transit resonance is included and the perturbed density response for the ions becomes

$$n_i = n\frac{e\phi}{T_e}\left\{-\tau + \frac{\omega_{*i}\omega}{k_\parallel^2 v_{ith}^2} S_0 \eta_i \right.$$

$$\left. + S_0 Z\left(\frac{\omega}{k_\parallel v_{ith}}\right)\left[-\frac{\tau\omega}{k_\parallel v_{ith}} + \frac{\omega_{*i}}{k_\parallel v_{ith}}\left(1 + \eta_i \frac{\omega^2}{k_\parallel^2 v_{ith}^2} - \frac{\eta_i}{2} - \eta_i bG\right)\right]\right\} \quad \cdots (1.1)$$

where $Z(\omega/k_\parallel v_{ith})$ is the plasma dispersion function, $b = (k_y\rho_i)^2$, $S_0 = \exp(-b)\, I_0(b)$, and $G=1-I_1(b)/I_0(b)$ with I_0 and I_1 being the zeroth and first order modified Bessel functions. The perturbed electron density is $n_e = ne\phi/T_e$. From quasi-neutrality, the dispersion relation can be written as

$$1 + \tau - \frac{S_0 \eta_i \omega_{*i}\omega}{k_\parallel^2 v_{ith}^2} - S_0 Z\left(\frac{\omega}{k_\parallel v_{ith}}\right)\left[-\frac{\tau\omega}{k_\parallel v_{ith}} + \frac{\omega_{*i}}{k_\parallel v_{ith}}\left(1 + \frac{\eta_i \omega^2}{k_\parallel^2 v_{ith}^2} - \frac{\eta_i}{2} - \eta_i bG\right)\right] = 0$$

which yields a necessary instability condition:

$$\eta_i > \frac{2}{1+2bG}$$

Again, the mode becomes unstable when η_i is higher than the above threshold value.

1.5. Plan of the thesis

The structure of this thesis is as fellows. In Chapter 2, the physics of ITG instability is reviewed briefly and the gyrokinetic formalism is established as a starting point. In Chapter 3, anisotropic effect of ion temperature gradient on the slab ITG mode

with collisions is studied. The results are then extended to the toroidal ITG limit in Chapter 4. In Chapter 5, a mixed slab and toroidal ITG mode is considered for the more realistic case. In Chapter 6, non-local effect is discussed. Finally, a summary is given in Chapter 7.

CHAPTER 2

PHYSICS OF ITG INSTABILITIES AND BASIC NEW FORMALISM

In the first part of this chapter, the physical mechanism of the ITG instability is reviewed briefly with emphasis on the anisotropic effect of ion temperature gradient. Both fluid and kinetic descriptions are given. In the second part, the gyrokinetic formalism is used to derive an expression for perturbed ion and electron densities by including anisotropic ion temperature gradient.

2.1 Physics of the ITG instability

2.1.1 Fluid Description

Consider the plasma as a compressible fluid with radial gradients in parallel and perpendicular temperatures. The purpose here is to find which temperature gradient is crucial to trigger the ITG instability.

The configuration is shown in Fig. 2.1. The uniform magnetic field **B** is in the +z-direction. Gradients in density and temperature are in the -x-direction. An electrostatic wave is launched with the wavevector **k**, electric field E_z and E_y. Due to E_z, plasma can be compressed along the magnetic field line producing ion acoustic type

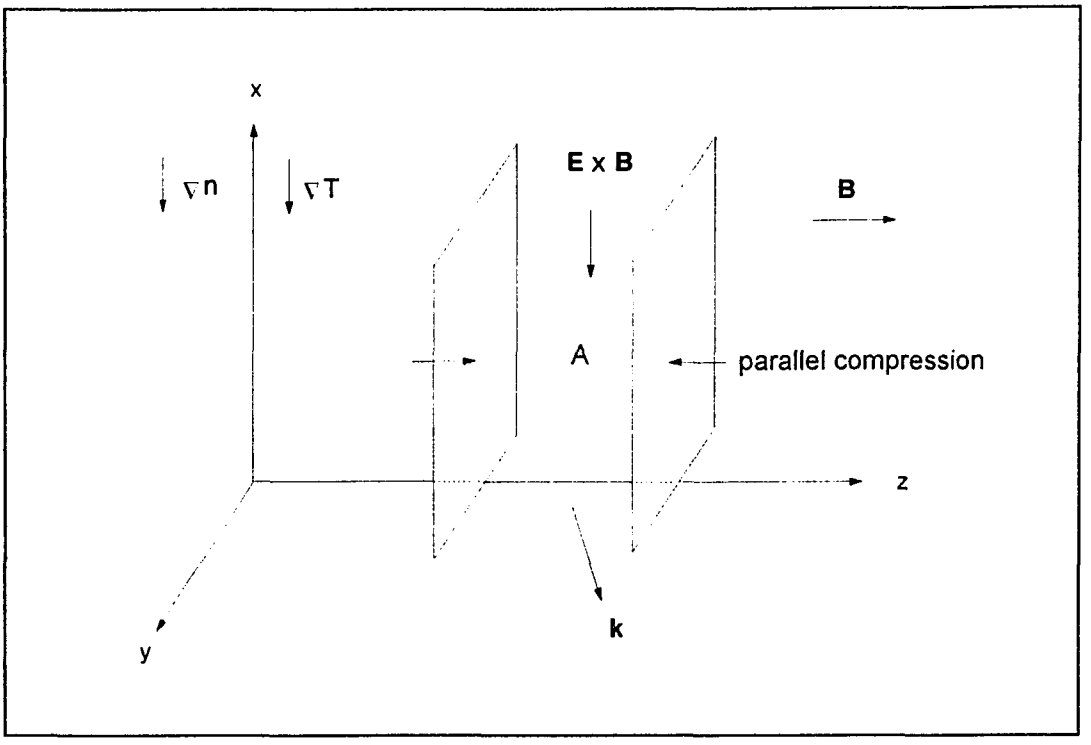

2.1 Diagram for the ITG instability for a fluid model

perturbation. Due to the electric field E_y, plasma can be moved up and down by the **E**×**B** drift in the x-direction.

In the case where there are no temperature gradients, parallel compression leads to an increase in the local density in region A. Simultaneously, the **E**×**B** drift brings less dense plasma into this region and approximately cancels the density increase by parallel compression. Under this situation, the total pressure in region A cannot be lowered by parallel compression. However, with temperature gradients, the plasma brought into region A by the **E**×**B** drift also has a lower temperature. This causes the total pressure in this region to be lower and consequently enhances parallel compression.

Thus, the perturbation grows. Here, temperature gradient in the perpendicular direction can only change the pressure in the perpendicular direction and cannot enhance the parallel compression. It is the parallel temperature gradient that changes the pressure in the parallel direction and therefore triggers the ITG instability.

To estimate the critical value of the parallel temperature gradient, the two fluid equations

$$\frac{\partial P}{\partial t} = -\vec{v}\cdot\nabla P - \Gamma P \nabla\cdot\vec{v}$$

$$\frac{\partial n}{\partial t} = -\vec{v}\cdot\nabla n - n\nabla\cdot\vec{v} \sim 0$$

are used to obtain the following equation

$$\frac{\partial P}{\partial t} = -(\Gamma - 1 - \eta_i) P \nabla\cdot\vec{v}$$

where n is the density, P is the pressure, $\eta_i \equiv \nabla \ln T_i / \nabla \ln n$, and $\Gamma = (d+2)/d$ is the ideal gas compressibility constant and d is the number of degrees of freedom. From the above discussion, η_i should be $\eta_{i\|} \equiv \nabla \ln T_{i\|} / \nabla \ln n$. Because the condition for negative compression is $\Gamma - 1 - \eta_{i\|} < 0$, a critical parallel temperature gradient $\eta_{i\|} = \Gamma - 1$ is thus obtained. In particular, for three-dimensional plasmas (d=3), $\Gamma = 5/2$ and $\eta_{i\|} = 2/3$.

2.1.2 Kinetic Description

The fluid description is simple and is used widely to explain the ITG instability.

However, it cannot be applied to the case where the instability is related to the wave-particle interaction. This interaction is especially strong near resonance $\omega = \mathbf{k}\cdot\mathbf{v}$, where $\mathbf{v}$ is the velocity of the particle that participates in the resonance. The resonant effect must be dealt with by the kinetic approach.

In the kinetic description, the ITG modes can be driven unstable by two kinds of driving forces: (1) due to the coupling of the parallel transit of the ions with the temperature gradient in the slab limit, (2) due to the coupling of the curvature and grad-B drift with the temperature gradient in the toroidal limit.

In the slab case, the guiding center of the ions only moves along the magnetic field lines and so transit resonance arises when the parallel velocity of the ions matches the parallel phase velocity of the mode: $\omega = k_{\parallel}v_{\parallel}$. Because $v_{\parallel}$ can be either positive

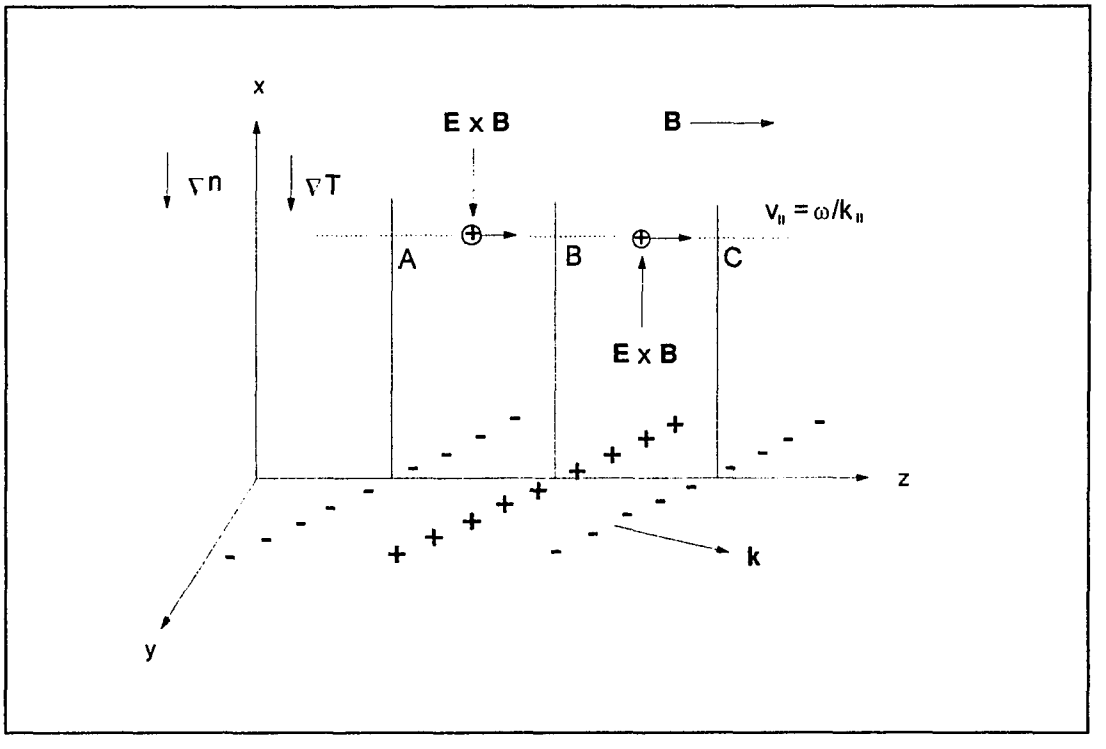

Fig. 2.2 Diagram for ITG instability for a kinetic model

or negative, the condition of transit resonance can always be satisfied for any frequency ω. The configuration shown in Fig.2.2 is similar to the one in the fluid situation except that the fluid is replaced now by resonant ions. The ions from A to B gain energy from the wave because they are accelerated by the perturbed parallel electric field **E**. These ions from A to B are brought there by **E**×**B** drift from a region where the temperature and density are lower. On the other hand, the ions from B to C which lose energy to wave originate from a region with a higher temperature and density. The energy gain may not balance the energy loss. This results in a net energy exchange between the wave and resonant ions. Thus, the wave can be driven unstable by the free energy. Specifically, the ITG instability arises either when energy is transferred to the positive energy wave or energy is extracted from the negative energy wave. To examine which temperature gradient is important, the number density of resonant particle at position x is noted to be

$$N_{res} \propto \frac{n(x)}{T_{\|}(x)^{1/2}} \exp\left[-\frac{m}{2T_{\|}(x)}\left(\frac{\omega}{k_{\|}}\right)^2\right]$$

since it relates to the amount of energy exchange. Note that the number of resonant particles is independent of the perpendicular temperature after the Maxwellian distribution function is integrated over the perpendicular velocity. By taking into account the number of the ions from A to C, the energy exchange is found to be only dependent on parallel temperature gradient. Again, in the kinetic description, parallel temperature gradient is crucial.

In the toroidal case, the wave is also driven unstable by the energy exchange between the wave and the resonant ions. However, there are two features that are different from the slab case. First, the guiding center now moves in the perpendicular

direction because the magnetic drift (magnetic curvature and grad-B drifts) is in the cross field direction. Second, the resonance condition becomes $\omega = k_y v_D$, where v_D is the magnetic drift velocity in y-direction. For bad magnetic curvature $v_D = -1/(\omega_c R)(v_{\parallel}^2 + v_{\perp}^2/2) < 0$ with R the major radius, only the mode propagating in the ion diamagnetic direction ($\omega<0$) can participate in the resonance. Since the drift velocity is dependent on both $v_{\parallel}$ and $v_{\perp}$, the marginal stability condition should be also dependent on both parallel and perpendicular temperature gradients.

2.2 Gyrokinetic formalism

From the physical point of view presented above, the incorporation of anisotropic temperature gradients for the analysis of the ITG instability is shown to be natural. Now anisotropic temperature gradient is brought into the analysis quantitatively. Instead of using the method of characteristics (MIYAMOTO, 1980), a gyrokinetic formalism (TAYLOR *et al.*, 1968) is employed here because of its elegant way to deal with the problem. In general, both transit and magnetic drift resonances can exist simultaneously and so they are included together in this derivation with anisotropic temperature gradients.

The distribution function for the steady state is considered to be a Maxwellian. Since density and temperature are not constant, the Maxwellian distribution can be expanded to lowest order in density and temperature gradients as follows:

$$F=F_M\left\{1-\frac{1}{L_n}\left(\frac{v_y}{\omega_c}+x\right)\left[1+\eta_{i\perp}\left(\frac{v_{\perp}^2}{2v_{\perp 0}^2}-1\right)+\eta_{i\parallel}\left(\frac{v_{\parallel}^2}{v_{ith}^2}-\frac{1}{2}\right)\right]\right\} \quad \cdots(2.1)$$

where F_M is the Maxwellian distribution function, $L_n \equiv -(d\ln n/dx)^{-1}$ is the density scale

length , $\eta_{i\perp} \equiv d\ln T_{i\perp}/d\ln n$, $\eta_{i\parallel} \equiv d\ln T_{i\parallel}/d\ln n$, $v_{ith} = (2T_{i\parallel}/m_i)^{1/2}$, and $v_{\perp 0} = (T_{i\perp}/m_i)^{1/2}$.

The electric potential has the form $\phi \exp(-i\omega t + ik_\parallel + ik_y)$. The perturbed distribution function f is also proportional to $\exp(-i\omega t + ik_\parallel + ik_y)$. In the electrostatic limit, the perturbed distribution function satisfies the Vlasov equation

$$-i\omega f + i\left(k_\parallel v_\parallel + k_y v_\perp \cos\psi + k_y v_D\right) f - \omega_c \frac{\partial f}{\partial \psi} = C(f, F)$$

$$= ie\phi F_M \left\{ -\frac{k_\parallel v_\parallel}{T_{i\parallel}} - \frac{k_y v_\perp \cos\psi}{T_{i\perp}} - \frac{k_y}{m_i L_n \omega_c}\left[1 + \eta_{i\perp}\left(\frac{mv_\perp^2}{2T_{i\perp}} - 1\right) + \eta_{i\parallel}\left(\frac{mv_\parallel^2}{2T_{i\parallel}} - \frac{1}{2}\right)\right]\right\}$$

where $\psi \equiv \tan^{-1}(v_x/v_y)$, C(f, F) is the collisional operator. Suppose that the equilibrium varies over some characteristic length scale L much larger than an ion Larmor radius $\rho_i = v_{\perp 0}/\omega_c$. Expand the perturbed distribution function $f = f_0 + f_1 + \cdots$ in the order of ρ_i/L. The lowest-order Vlasov equation for the perturbations is

$$i\frac{k_y v_\perp \cos\psi}{\omega_c} f_0 - \frac{\partial f_0}{\partial \psi} = -i\frac{e\phi}{T_{i\perp}} \frac{k_y v_\perp \cos\psi}{\omega_c} F_M ,$$

which yields

$$f_0 = h_i \exp\left(i\frac{k_y v_\perp}{\omega_c}\sin\psi\right) - \frac{e\phi}{T_{i\perp}} F_M ,$$

where h_i is yet to be determined by the following next-order Vlasov equation for the perturbations

$$-i\omega f_0+i\left(k_{\parallel}v_{\parallel}+k_y v_D\right) f_0+ik_y v_{\perp}\cos\psi f_1-\omega_c\frac{\partial f_1}{\partial\psi}-C(f,F)$$

$$=ie\phi F_M\left\{-\frac{k_{\parallel}v_{\parallel}}{T_{i\parallel}}-\frac{k_y}{m_i L_n\omega_c}\left[1+\eta_{i\perp}\left(\frac{mv_{\perp}^2}{2T_{i\perp}}-1\right)+\eta_{i\parallel}\left(\frac{mv_{\parallel}^2}{2T_{i\parallel}}-\frac{1}{2}\right)\right]\right\}$$

Substituting f_0 into the above equation, an equation for h_i is obtained as

$$\left(\omega-k_{\parallel}v_{\parallel}-k_y v_D\right) h_i-iC(f,F)\exp\left(-i\frac{k_y v_{\perp}}{\omega_c}\sin\psi\right)$$

$$=i\omega_c\frac{\partial}{\partial\psi}\left[f_1\exp\left(-i\frac{k_y v_{\perp}}{\omega_c}\sin\psi\right)\right]+\exp\left(-i\frac{k_y v_{\perp}}{\omega_c}\sin\psi\right)$$

$$\times e\phi F_M\left\{\frac{\omega}{T_{i\perp}}+\frac{k_{\parallel}v_{\parallel}}{T_{i\parallel}}-\frac{k_{\parallel}v_{\parallel}}{T_{i\perp}}+\frac{k_y}{m_i L_n\omega_c}\left[1+\eta_{i\perp}\left(\frac{v_{\perp}^2}{2v_{\perp 0}^2}-1\right)+\eta_{i\parallel}\left(\frac{v_{\parallel}^2}{v_{ith}^2}-\frac{1}{2}\right)\right]\right\}$$

The first term of the RHS of the equation is the only term related to f_1 and it vanishes after averaging over the gyrophase angle ψ. Then, the equation for perturbed distribution f_0 is truncated. Using the Krook collisional operator $C(f, F) = -\nu_i h_i \exp(ik_y v_{\perp}\sin\psi/\omega_c)$ (BHATNAGAR *et al.*, 1954) with ν_i the ion collision frequency, h_i can be solved as

$$h_i=e\phi F_M J_0\left(\frac{k_y v_{\perp}}{\omega_c}\right)$$

$$\times \frac{\left\{ \frac{\omega}{T_{i\perp}} + \frac{k_\parallel v_\parallel}{T_{i\parallel}} - \frac{k_\parallel v_\parallel}{T_{i\perp}} + \frac{k_y}{m_i L_n \omega_c} \left[1 + \eta_{i\perp} \left(\frac{m v_\perp^2}{2 T_{i\perp}} - 1 \right) + \eta_{i\parallel} \left(\frac{m v_\parallel^2}{2 T_{i\parallel}} - \frac{1}{2} \right) \right] \right\}}{\omega + i\nu_i - k_\parallel v_\parallel - k_y v_D}$$

where

$$\frac{1}{2\pi} \int_0^{2\pi} d\psi \; \exp\left(-i \frac{k_y v_\perp}{\omega_c} \sin\psi \right) = J_0\left(\frac{k_y v_\perp}{\omega_c} \right)$$

is the zeroth-order Bessel function. Here, the Bessel function comes from the effect of the finite Larmor radius (FLR). By using the dimensionless parameters $p = v_\parallel / v_{ith}$, $u = (v_\perp / v_{\perp 0})^2$, $\tau_\parallel = T_e / T_{i\parallel}$, $\tau_\perp = T_e / T_{i\perp}$, $\varepsilon_n \equiv L_n / R$, $b = (k_y \rho_i)^2$, $\omega_{*i} = -(\tau_\parallel \tau_\perp / 2)^{1/2} k_y \rho_i$, and $\omega_D = -\varepsilon_n k_y \rho_i (\tau_\parallel / 2\tau_\perp)^{1/2}$, h_i can be rewritten as

$$h_i = \frac{n}{2\pi^{3/2} v_{ith} v_{\perp 0}^2} \left(\frac{e\phi}{T_e} \right) \exp(-p^2 - u/2) \, J_0(\sqrt{bu})$$

$$\times \frac{\omega\tau_\perp + k_\parallel p(\tau_\parallel - \tau_\perp) - \omega_{*i} \left[1 + \eta_{i\perp}(u/2 - 1) + \eta_{i\parallel} (p^2 - 1/2) \right]}{\omega + i\nu_i - k_\parallel p - \omega_D (u/2 + 2\tau_\perp p^2 / \tau_\parallel)}$$

where $k_\parallel$ has been normalized to $1/L_n$, ω and ν_i have been normalized to v_{ith}/L_n. Finally, the perturbed ion density can be expressed as

$$n_i = \int d\vec{v} \; f_0$$

$$= n \frac{e\phi}{T_e} \left[-\tau_\perp + \left\langle \frac{\omega\tau_\perp + k_\parallel p(\tau_\parallel - \tau_\perp) - \omega_{*i} \left[1 + \eta_{i\perp}(u/2 - 1) + \eta_{i\parallel} (p^2 - 1/2) \right]}{\omega + i\nu_i - k_\parallel p - \omega_D (u/2 + 2\tau_\perp p^2 / \tau_\parallel)} \right\rangle \right] \quad \cdots (2.2)$$

where

$$\langle \cdots \rangle = \frac{1}{2\sqrt{\pi}} \int_{-\infty}^{+\infty} dp \int_{0}^{+\infty} du \, \exp(-p^2 - u/2) \, J_0^2(\sqrt{bu}) \, (\cdots)$$

is a velocity average over a Maxwellian.

By using the same procedure, the perturbed density for electron can also be obtained as

$$n_e = n \frac{e\phi}{T_e} \left[1 - \left\langle \frac{\omega - \omega_{*e} \left[1 + \eta_e (u/2 - 1) + \eta_e \, (p^2 - 1/2) \right]}{\omega + i\nu_e - \sqrt{\tau_\parallel m_i / m_e} k_\parallel p} \right\rangle \right] \quad \cdots (2.3)$$

where for electron $\eta_e \equiv d\ln T_e / d\ln n$, $u = m_e v_\perp^2 / T_e$, $p^2 = m_e v_\parallel^2 / 2T_e$ and $\omega_{*e} = -\omega_{*i}$ and

$$\langle \cdots \rangle = \frac{1}{2\sqrt{\pi}} \int_{-\infty}^{+\infty} dp \int_{0}^{+\infty} du \, \exp(-p^2 - u/2) \, (\cdots) \, .$$

Note that the electron collisional frequency ν_e has also been normalized to v_{ith}/L_n.

In summary, the perturbed densities of ion and electron given by Eqs. (2.2) and (2.3) are finally obtained by using the gyrokinetic formalism. The anisotropic ion temperature gradients are included in these expressions. These results are subsequently used in the following chapters.

CHAPTER 3

SLAB ITG INSTABILITY WITH ANISOTROPIC ION TEMPERATURE GRADIENT

The effect of anisotropic ion temperature gradients on the slab ITG instability was investigated by Mathey and Sen (MATHEY *et al.*, 1989). In their work, they suggested a possible stabilization scheme for the slab ITG mode. Assuming that the mode is damped at a constant rate, they showed that the threshold value of a gradient in the parallel ion temperature can be significantly increased for a large gradient in the perpendicular ion temperature. The study in this chapter improves on their model. Instead of using the *ad hoc* damping, a realistic damping effect is considered to obtain the criterion for the slab ITG instability.

The effect of the dissipative trapped electrons is investigated as a possible candidate of the realistic damping. Since the effective collision frequency is usually lower than the bounce frequency for both electrons and ions in present day tokamaks, particles may thus be trapped in the local magnetic well. The following frequency ordering is assumed:

$$\omega_{te}, \omega_{be} > \nu_{eff,e} \gg |\omega|, \omega_{ti} > \omega_{bi} > \nu_{eff,i}$$

where ω_b is the bounce frequency, ω_t is the transit frequency, ν_{eff} is the effective

collision frequency, and the subscripts 'e' and 'i' stand for the electron and ion species, respectively. Under this frequency ordering, trapped electrons experience many bounce oscillations and collisions during one wave period. However, the bounce frequency for trapped ions is considered to be so low that bounce oscillations can be neglected during one wave period and the trapped ions behave approximately as transit ions. The above inequality also gives the frequency ordering for transit particles. For transit ions no approximation is made while for transit electrons the adiabatic response can be used due to the high transit frequency.

3.1. Dispersion relation

In the slab limit, only the transit resonance is taken into account. The magnetic drift resonance is neglected by taking $v_D = 0$. Because the bounce motion for trapped ions is not important under the frequency ordering, all ions can be considered as transit ions. From Eq. (2.2), the perturbed density of ions can be written as

$$n_i = n\frac{e\phi}{T_e}\left[-\tau_\perp + \left\langle \frac{\omega\tau_\perp + k_\parallel p(\tau_\parallel - \tau_\perp) - \omega_{*i}\left[1+\eta_{i\perp}(u/2-1)+\eta_{i\parallel}(p^2-1/2)\right]}{\omega + iv_i - k_\parallel p} \right\rangle\right] \cdots (3.1)$$

After integrating over the velocity space, an analytical expression of n_i can be obtained as

$$n_i = n\frac{e\phi}{T_e}\left\{-\tau_\perp + S_0(\tau_\perp - \tau_\parallel) + \left(\frac{\omega_{*i}}{k_\parallel}\right)\left(\frac{\omega + iv_i}{k_\parallel}\right)S_0\eta_{i\parallel}\right.$$

$$+S_0 Z\left(\frac{\omega+i\nu_i}{k_\parallel}\right)\left[-\tau_\parallel\frac{\omega}{k_\parallel}+i\frac{\nu_i}{k_\parallel}(\tau_\perp-\tau_\parallel)+\frac{\omega_{*i}}{k_\parallel}\left(1+\eta_{i\parallel}\frac{(\omega+i\nu_i)^2}{k_\parallel^2}-\frac{\eta_{i\parallel}}{2}-\eta_{i\perp}bG\right)\right]\Bigg\}$$

In the limit of $\nu_i = 0$ and $\eta_{i\parallel} = \eta_{i\perp} = \eta_i$, this result recovers Eq. (1.1).

Trapped electrons oscillate in a local magnetic well with maximum magnetic field $B_{max} = B_0$ and minimum $B_{min} = B_0$ (1-r/R), where r is the toroidal minor radius. From the invariance of the magnetic moment and the conservation of energy, the trapping condition can be stated as $v_\parallel^2 < v_\perp^2[r/R(1-r/R)] \sim v_\perp^2 r/R$ for small r/R. By integrating the Maxwellian distribution over this velocity space for the trapped electrons, the trapped fraction $n_{trap}/n = \varepsilon^{1/2}$ is thus obtained, where $\varepsilon \equiv r/R$. Based on this result, the following approximation is often used to simplify the calculation for the perturbed density of trapped electrons:

$$\int_{trap} d\vec{v} \sim \sqrt{\epsilon}\int d\vec{v}$$

The calculation is further simplified by noticing that $\nu_{eff,e} >> \omega$ and that the FLR effect can be neglected for electrons. Finally, the perturbed density for trapped electrons becomes

$$n_{et}=\sqrt{\epsilon}n\frac{e\phi}{T_e}$$

$$\times\left[1+\frac{i}{2\sqrt{\pi}}\int_{-\infty}^{+\infty}dp\int_0^{+\infty}du\,\exp(-p^2-u/2)\,\frac{\omega-\omega_{*e}\left[1+\eta_e(u/2-1)+\eta_e(p^2-1/2)\right]}{\nu_{eff,e}}\right].$$

where $\nu_{eff,e}$ is the effective collision frequency for trapped electrons. Using a velocity dependent collision frequency $\nu_{eff,e} = (\nu_e/\varepsilon)(p^2 + u/2)^{-3/2}$, the perturbed electron density

reduces to

$$n_{et}=n\frac{e\phi}{T_e}\left(\sqrt{\epsilon}+i\frac{4\epsilon^{3/2}}{\sqrt{\pi}\nu_e}\left[\omega-\omega_{*e}(1+1.5\eta_e)\right]\right).$$

By including the adiabatic response of transit electrons $n_{eu} = (1 - \varepsilon^{1/2})ne\phi/T_e$, the perturbed density of electrons becomes

$$n_e=n\frac{e\phi}{T_e}(1-i\delta) \quad \cdots(3.2)$$

where

$$\delta=-\frac{4\epsilon^{3/2}}{\sqrt{\pi}\nu_e}\left[\omega-\omega_{*e}(1+1.5\eta_e)\right].$$

From Poisson's equation $\nabla\cdot\mathbf{E} = 4\pi\rho$, the dielectric function can be written as

$$D(\omega)=1+\frac{1-i\delta+\tau_\perp-\langle\cdots\rangle}{k^2\lambda_e^2}$$

where $k^2 =(k_\parallel^2/L_n^2) + (k_y^2/\rho_i^2)$, λ_e is the electron Debye length, and $\langle\cdots\rangle$ is the non-adiabatic response in Eq. (3.1). For $k\lambda_e << 1$, the quasi-neutrality condition $n_e = n_i$ holds, yielding the following dispersion relation:

$$1-i\delta+\tau_\perp-S_0(\tau_\perp-\tau_\parallel)-\left(\frac{\omega_{*i}}{k_\parallel}\right)\left(\frac{\omega+i\nu_i}{k_\parallel}\right)S_0\eta_{i\parallel}-S_0Z\left(\frac{\omega+i\nu_i}{k_\parallel}\right)$$

$$\times\left\{-\tau_\parallel\frac{\omega}{k_\parallel}+i\frac{\nu_i}{k_\parallel}(\tau_\perp-\tau_\parallel)+\left(\frac{\omega_{*i}}{k_\parallel}\right)\left[1+\eta_{i\parallel}\left(\frac{\omega+i\nu_i}{k_\parallel}\right)^2-\frac{\eta_{i\parallel}}{2}-\eta_{i\perp}bG\right]\right\}=0 \quad \cdots(3.3)$$

3.2. Collisionless slab ITG instability

In the collisionless limit ($\delta = 0$ and $\nu_i = 0$), the left side of the above dispersion relation contains real and imaginary parts and so two equations can be obtained from the dispersion relation. At marginal stability $\gamma = 0$, where γ is the growth rate, the real frequency can be solved as

$$\frac{\omega}{k_\parallel} = \left(\frac{k_\parallel}{\omega_{*i}\eta_{i\parallel}}\right)\left(\tau_\parallel - \tau_\perp + \frac{1+\tau_\perp}{S_0}\right) \quad \cdots(3.4)$$

The other equation gives a relation between $\eta_{i\perp}$ and $\eta_{i\parallel}$

$$\eta_{i\parallel} = 1 - \eta_{i\perp} bG \pm \left[(1-\eta_{i\perp} bG)^2 + \frac{2k_\parallel^2}{\omega_{*i}^2}\left(\tau_\parallel - \tau_\perp + \frac{1+\tau_\perp}{S_0}\right)\left(-\tau_\perp + \frac{1+\tau_\perp}{S_0}\right)\right]^{1/2} \quad \cdots(3.5)$$

which is simply the marginal stability boundary in the $\eta_{i\perp}$-$\eta_{i\parallel}$ plane. Here, the upper (lower) sign gives a positive (negative) threshold value of $\eta_{i\parallel}$ corresponding to the wave propagating in the ion (electron) diamagnetic direction. These results are plotted in Fig. 3.1(a) and (b). It is shown that the parallel temperature gradient is crucial to trigger the instability. However, the marginal stability condition is not uniquely determined by the parallel temperature gradient. The perpendicular temperature gradient is also involved through the FLR effect. The physical reason for this is discussed as follows.

Figure 3.2 is used to explain the situation. The resonant ions move in the +z-direction when $\omega > 0$. Due to the **E**×**B** drift in the x-direction, the ions at position A are actually brought there from a position $x + \delta t E_y c/B$ within the time interval δt. Due to resonant interaction, the ions are also slowed down from $v_\parallel + \delta t e E_\parallel / m_i$ to $v_\parallel$. For

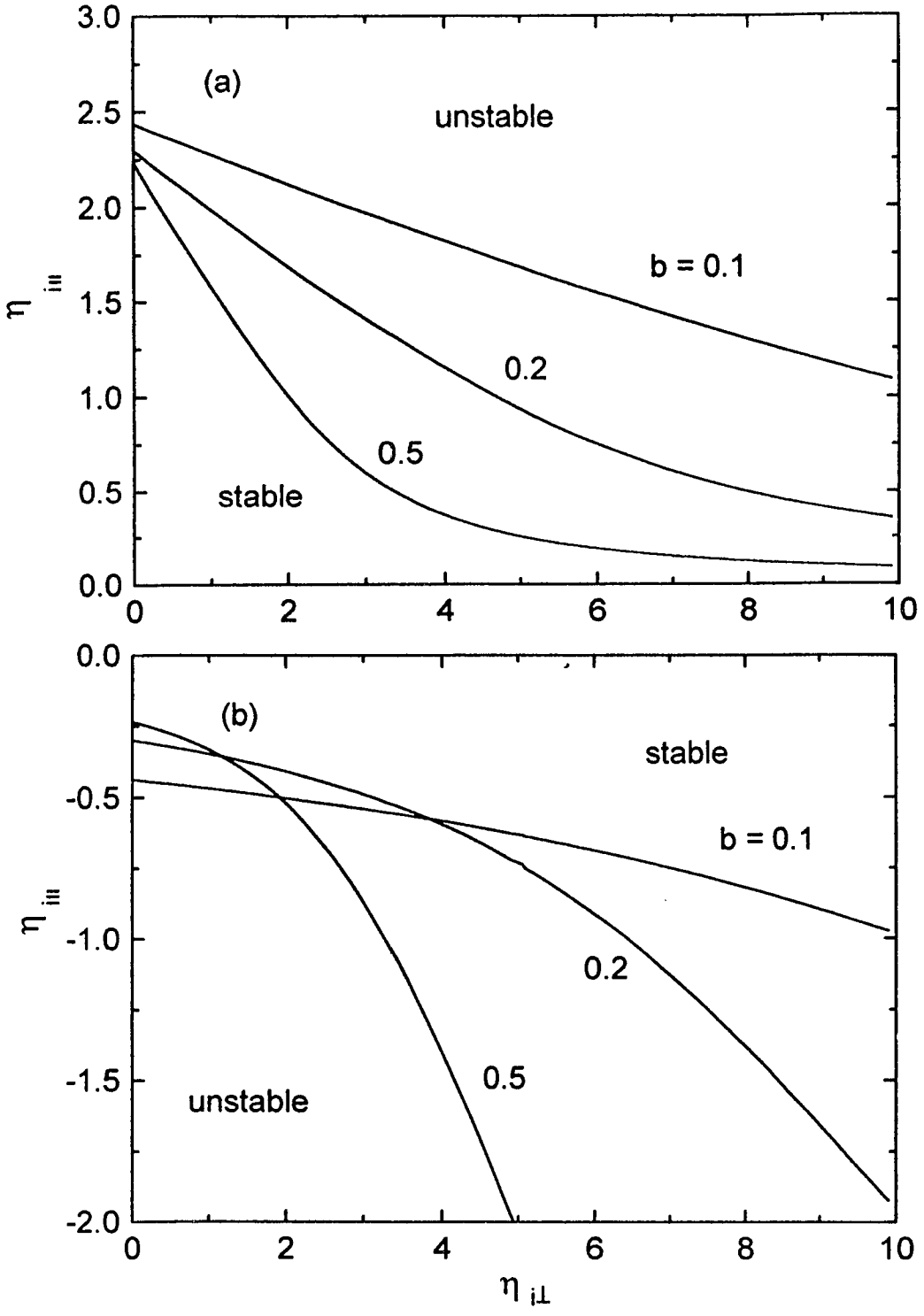

Fig. 3.1. The marginal stability boundaries in the $\eta_{i\perp}$-$\eta_{i\parallel}$ plane for $\tau_\perp = \tau_\parallel = 1$, $k_\parallel L_n = 0.1$ (a) for the slab ion branch and (b) for the slab electron branch.

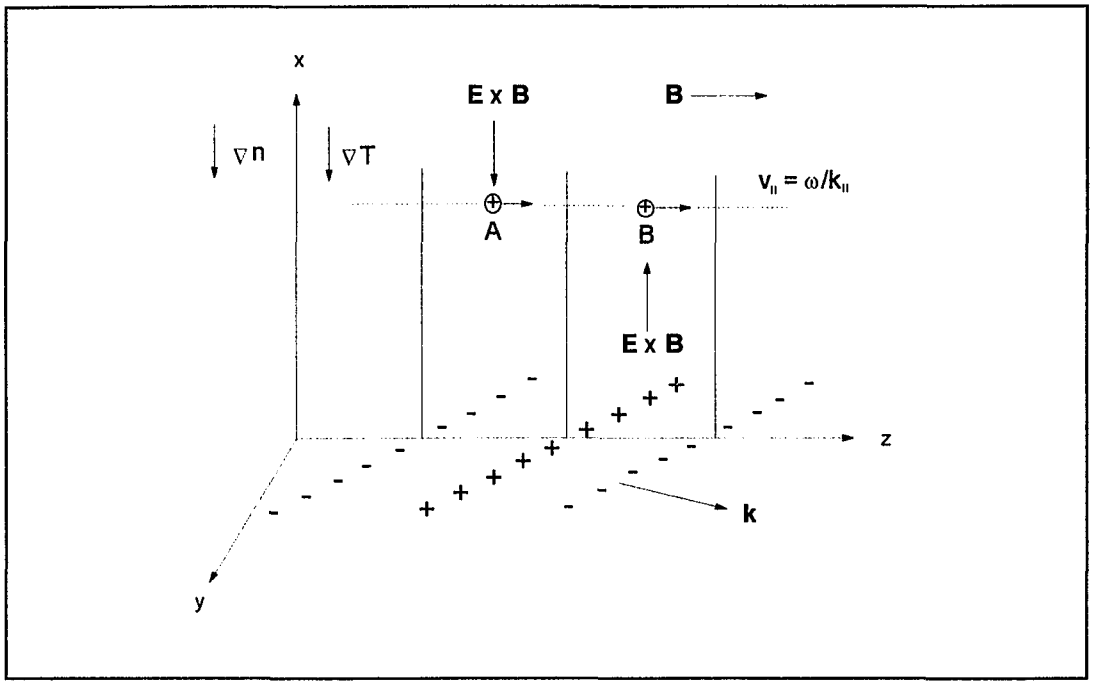

Fig. 3.2 Slab ITG instability

these ions, the power density transferred from the resonant ions to the wave can be written as

$$P_A = \int d\vec{v}\ eE_{\parallel} v_{\parallel} F_h\left(x + \delta t \frac{E_y C}{B},\ v_{\parallel} + \delta t \frac{eE_{\parallel}}{m_i}\right)$$

where the distribution function $F_h(x, \mathbf{v}) = S_0(b)F(x, \mathbf{v})$ includes the FLR effect. The ions at B gain energy from the wave and so the power density transferred to the wave is

$$P_B = -\int d\vec{v}\ eE_{\parallel} v_{\parallel} F_h\left(x - \delta t \frac{E_y C}{B},\ v_{\parallel} - \delta t \frac{eE_{\parallel}}{m_i}\right)$$

The total power density $P = P_A + P_B$ is then given by

$$P=2\int d\vec{v}\ eE_{\parallel}v_{\parallel}\left(\frac{\partial F_b}{\partial x}\delta t\frac{E_y C}{B}+\frac{\partial F_b}{\partial v_{\parallel}}\delta t\frac{eE_{\parallel}}{m_i}\right)$$

Here, $\partial F_b/\partial v_{\parallel} = -2v_{\parallel}/v_{ith}^2 F_M$ and $\partial F_b/\partial x$ has two contributions: one is from $\partial F/\partial x$ which can be obtained from Eq. (2.1), the other is from the FLR effect. Because the Larmor radius is also a function of x, we have $\partial S_0/\partial x = -S_0 Gb\partial \ln T_{\perp}/\partial x$. The integration over the parallel velocity is only from the resonant ions within a parallel velocity range $\Delta v_{\parallel} \sim (\pi/4k_{\parallel})\delta t$. After some manipulations, the power density transferred to the wave becomes

$$P=\frac{\sqrt{\pi}S_0 ne^2 E_{\parallel}^2 v_{ith}L_n}{2T_e k_{\parallel}^2}\exp(-\omega^2/k_{\parallel}^2)$$

$$\times\left\{-\tau_{\parallel}\frac{\omega^2}{k_{\parallel}}+\left(\frac{\omega\omega_{*i}}{k_{\parallel}}\right)\left[1+\eta_{i\parallel}\left(\frac{\omega}{k_{\parallel}}\right)^2-\frac{\eta_{i\parallel}}{2}-\eta_{i\perp}bG\right]\right\} \quad \cdots(3.6)$$

This result is also true for the case of $\omega < 0$. The first term of the RHS in the above equation is related to the change in the parallel velocity of the resonant ions. It is always negative and so the power is transferred from the wave to the resonant ions. The other terms are related to the exchange of energy owing to the $\mathbf{E}\times\mathbf{B}$ drift. Among these terms, the third one corresponds to the variation in density. The fourth and fifth terms result from the change in parallel temperature. The last term, which contains the perpendicular temperature gradient, is obtained by considering that the Larmor radius (perpendicular temperature) varies with position x.

The total wave energy can be obtained by using $W_t = W_E d(\omega D_r(\omega))/d\omega$ with W_E being the electric field energy density. When $(\omega/k)^2$ is not too large, W_t is found to be

negative. The mode carries a negative energy because the total kinetic energy of the ions is less when the perturbation is present than when it is absent. A good example of this type of wave is the slow wave of the two-stream instability (HASEGAWA, 1975). The behavior of the negative energy wave is completely different. Usually, the first term of the RHS in Eq. (3.6) is the Laudau damping term. However, for the negative energy type of wave, it causes the wave to grow and now becomes an inverse Landau damping term. The second term is positive for the wave propagating in the ion diamagnetic direction ($\omega < 0$) but is negative for the wave propagating in the electron diamagnetic direction ($\omega > 0$). (Note $\omega_{*_i} < 0$) That is to say, the density gradient can stabilize the ion branch ($\omega < 0$) but destabilize the electron branch ($\omega > 0$). The terms related to parallel temperature gradient can be rewritten as

$$\eta_{i\parallel}\left(\frac{\omega}{k_\parallel}\right)^2 - \frac{\eta_{i\parallel}}{2} = \frac{k_\parallel^2}{\omega_{*i}^2 \eta_{i\parallel}}\left(\tau_\parallel - \tau_\perp + \frac{1+\tau_\perp}{S_0}\right)^2 - \frac{\eta_{i\parallel}}{2}$$

where Eq. (3.4) has been used to obtain the result. For the ion branch, an increase in $\eta_{i\parallel}$ leads to increase in the power transferred to the resonant ions. Because the wave has negative energy, large $\eta_{i\parallel}$ can destabilize the mode. The term with $\eta_{i\perp}$ is also negative and so large $\eta_{i\perp}$ also has a destabilizing effect. However, for the electron branch these terms with $\eta_{i\parallel}$ and $\eta_{i\perp}$change sign. In this case, the wave becomes more stable with increasing $\eta_{i\parallel}$ or $\eta_{i\perp}$.

3.3 . ITG instability with collisions

First consider a case without ion collisions $\nu_i = 0$. The real frequency at marginal stability is solved from the dispersion relation given by Eq. (3.3):

$$\frac{\omega}{k_\parallel}=\left(\frac{k_\parallel}{\omega_{*i}\eta_{i\parallel}}\right)\left(\tau_\parallel-\tau_\perp+\frac{1+\tau_\perp}{S_0}+\frac{Z_r\delta}{Z_iS_0}\right)$$

Substituting the frequency into the imaginary part of the dispersion relation given by Eq. (3.3), the following marginal stability boundary in the $\eta_{i\parallel}$-$\eta_{i\perp}$ plane is obtained

$$\eta_{i\parallel}=1-\eta_{i\perp}bG+\frac{k_\parallel\delta}{\omega_{*i}S_0Z_i}\pm\left[\left(1-\eta_{i\perp}bG+\frac{k_\parallel\delta}{\omega_{*i}S_0Z_i}\right)^2\right.$$

$$+\frac{2k_\parallel^2}{\omega_{*i}^2}\left(\tau_\parallel-\tau_\perp+\frac{1+\tau_\perp}{S_0}\right)\left(-\tau_\perp+\frac{1+\tau_\perp}{S_0}\right)$$

$$\left.+\frac{2k_\parallel^2Z_r\delta}{\omega_{*i}^2S_0Z_i}\left(\tau_\parallel-2\tau_\perp+\frac{2+2\tau_\perp}{S_0}+\frac{Z_r\delta}{Z_iS_0}\right)\right]^{1/2}$$

With the dissipative trapped electrons $\varepsilon>0$, both the upper and lower marginal stability boundaries are changed. The correction terms are proportional to $\delta/Z_i \sim \delta\exp(\omega^2/k_\parallel^2)$, which is significant for large $\omega^2/k_\parallel^2$. From the expression of real frequency of Eq. (3.4), large $\omega^2/k_\parallel^2$ can be reached for small absolute value of critical $\eta_{i\parallel}$. For the ion branch (the mode propagating in the ion diamagnetic direction), threshold $\eta_{i\parallel}$ is decreased with increasing $\eta_{i\perp}$ and so the effect of the dissipative electron is expected to have a significant influence at large threshold value of $\eta_{i\perp}$. For the electron branch (the mode propagating in the electron diamagnetic direction), the low absolute value of threshold $\eta_{i\parallel}$ can be obtained at small $\eta_{i\perp}$ and therefore electron collisions are expected to play an important role at small $\eta_{i\perp}$. For both situations, the power density due to the transit

resonance exponentially decays with $\omega^2/k_\parallel^2$ while the power dissipation due to electron collisions only varies with $\omega\delta$. That is why electron collisions become the dominant mechanism of energy exchange between the wave and ions when $\omega^2/k_\parallel^2 >> 1$.

The upper boundary (ion branch) is shown in Fig. 3.3(a) with parameters $\nu_{*e} = \nu_{eff,e}/\omega_{be} = 0.1$ and $\varepsilon^{1/2} = 0.32$, which are representative of a 'supershot' in TFTR (ZARNSTORFF *et al.*, 1989). It is seen that electron collisions have a stabilizing effect on the ion branch. The threshold value of the parallel ion temperature gradient is dramatically increased for large perpendicular temperature gradients and a large transverse wavenumber $b^{1/2}$. The reason is that the total wave energy becomes positive at large $\eta_{i\perp}$ and therefore electron collisions change their role and stabilize the mode. The marginal stability curve becomes non-monotonic and a second stability regime appears as in the work by Mathey (MATHEY *et al.*, 1989). However, the *ad hoc* damping in the reference is now replaced by the dissipative trapped electron dynamics. Significant stabilizing effect of this dynamics is found at large $\eta_{i\perp}$.

For the lower boundary (electron branch), the threshold values of the ion temperature gradient with the same parameters are shown in Fig. 3.3(b). Here, collisions also change their role when the total wave energy changes from a negative to a positive value. Now electron collisions have a destabilizing effect at small $\eta_{i\perp}$ because power density due to collisions changes sign for the electron branch. A surprising result is that the destabilizing effect on the electron branch is so dramatic that the threshold $\eta_{i\parallel}$ switches from a negative to a positive value for large b. To understand this, the dispersion relation can be expanded in the fluid-ion limit of $\omega/k_\parallel >> 1$ because this situation arises for large $\omega^2/k_\parallel^2$:

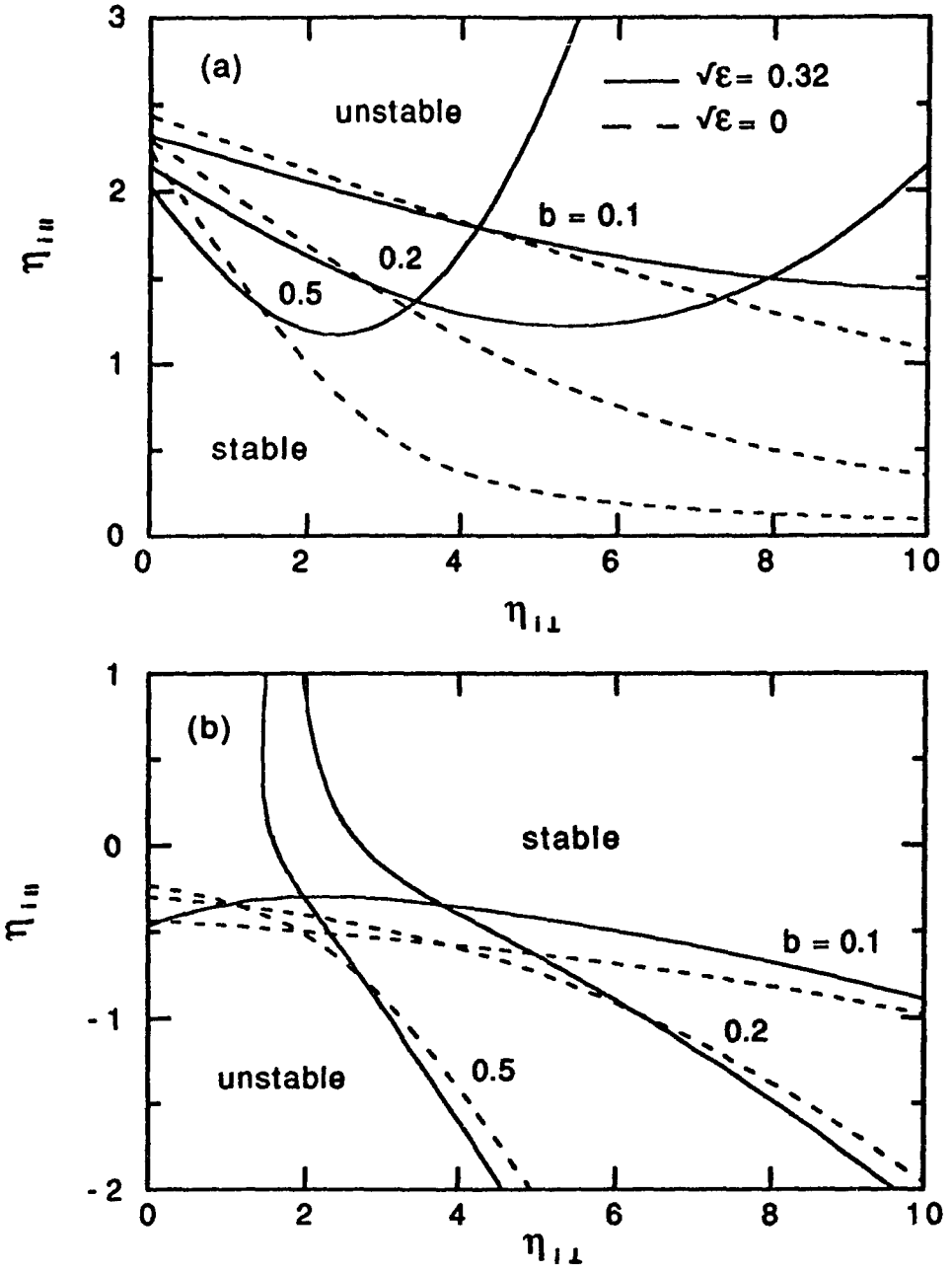

Fig. 3.3 The marginal stability boundaries in the $\eta_{i\parallel}$-$\eta_{i\perp}$ plane with electron collisions $\nu_{*_e} = 0.1$ when $\varepsilon^{1/2} = 0.32$, $\tau_\perp = \tau_\parallel = 1$, $k_\parallel L_n = 0.1$ and $2\pi L_n/L_b = 0.1$, with L_b the bounce length (a) for the slab ion branch and (b) for the slab electron branch.

$$1-i\delta+b\left(\tau_\perp-\frac{\omega_{*e}(1+\eta_{i\perp})}{\omega}\right)+i\sqrt{\pi}\frac{\omega_{*e}\omega^2\eta_{i\parallel}}{k_\parallel^3}\exp\left(-\frac{\omega^2}{k_\parallel^2}\right)=0$$

which yields

$$\omega=\omega_{*e}[1-b(1+\eta_{i\perp}-\tau_\perp)]$$

and

$$\gamma=\frac{4\omega_{*e}^2\sqrt{\epsilon}}{\sqrt{\pi}\nu_{eff,e}}[\eta_e+b(1+\eta_{i\perp}-\tau_\perp)]-\sqrt{\pi}\frac{\omega_{*e}^2\omega^2\eta_{i\parallel}}{k_\parallel^3}\exp\left(-\frac{\omega^2}{k_\parallel^2}\right)$$

This is the dissipative trapped electron mode with ion temperature gradients. For η_e = 0, the usual driving term in the growth rate vanishes. The second term on the right is the FLR and collisional contribution and can also destabilize the mode. The last term is related to the parallel temperature gradient. For negative $\eta_{i\parallel}$, it gives a destabilizing contribution. In order to satisfy the marginal stability condition γ = 0, $\eta_{i\parallel}$ must change to a positive value. Because $\exp(-\omega^2/k_\parallel^2) << 1$, a very large positive $\eta_{i\parallel}$ is needed to balance the destabilizing effect from the second term.

Now consider ion collisions. The ion collisionality is chosen to be $\nu_{*i} = \nu_{eff,i}/\omega_{bi}$ = 0.01 corresponding to the same TFTR case considered for electron collisions. The marginal stability diagram is shown in Fig. 3.4 for both the ion and electron branches. It indicates that ion collisions may slightly stabilize the slab ITG mode. However, the correction from ion collisions is so small that it can be neglected compared with that from electron collisions.

3.4. Conclusion

In the slab case, $\eta_{i\parallel}$ is crucial to trigger the ITG instability. $\eta_{i\perp}$ only becomes important when the FLR effect is taken into account. Two stability boundaries are found. For the ion branch, the threshold η_i is positive and increasing $\eta_{i\parallel}$ or $\eta_{i\perp}$ destabilizes the ITG mode. However, for the electron branch, the threshold η_i is negative and increasing $\eta_{i\parallel}$ or $\eta_{i\perp}$ stabilizes the mode. The difference between the ion and electron branches is

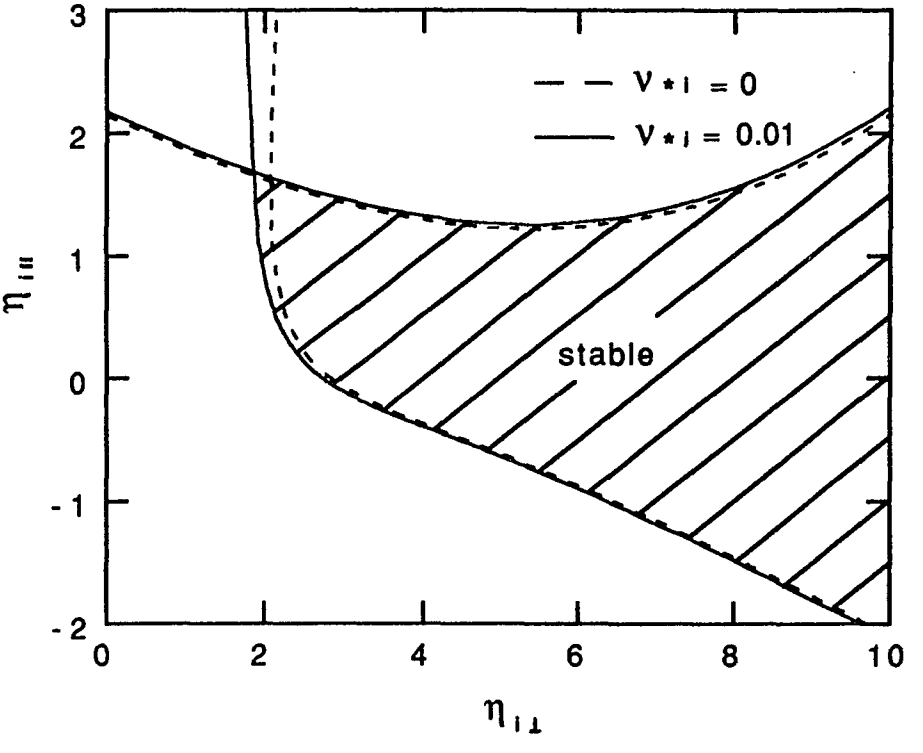

Fig. 3.4 The marginal stability boundaries including ion collisions $\nu_{*i} = 0.01$ when b = 0.2, $\varepsilon^{1/2} = 0.32$, $\tau_\perp = \tau_\parallel = 1$, $k_\parallel L_n = 0.1$ and $2\pi L_n/L_b = 0.1$.

related to the sign change in the power transferred to the wave due to the temperature gradients. Also, the power transfer to the wave due to collisions from dissipative trapped electrons is dependent on the direction of the propagation of the wave. When transit resonance is strong, dissipative trapped electrons have a negligible destabilizing (stabilizing) effect on the ion (electron) branch. However, for weak transit resonance, the total energy of the wave changes from a negative to a positive value. Therefore, collisions from dissipative trapped electrons significantly stabilize (destabilize) the ion (electron) branch.

CHAPTER 4

TOROIDAL ITG INSTABILITIES

There are two parts of this chapter. In the first part, the study of the ITG instability is extended to the toroidal limit by replacing the transit resonance with the magnetic drift resonance. In the slab case, it was found that collisions from the dissipative trapped electrons played an important role and therefore this effect is also included here. The collisionless case was investigated by Kim *et al.* (KIM *et al.*, 1991). They found that either a parallel or perpendicular temperature gradient could have a destabilizing effect. However, their work only covered the mode propagating in the electron diamagnetic direction. The study in this part shows that the ion branch can also be responsible for the toroidal ITG instability. The ion branch is important because the magnetic drift resonance only exists for this branch.

In the second part, a different version of the instability called the trapped ion ITG mode is investigated with anisotropic temperature gradients and collisions. This mode is used to correlate the present study with a recent experiment (ZARNSTORFF *et al.*, 1991). Unlike the other numerical studies (XU *et al.*, 1991, DONG *et al.*, 1992, KIM *et al.*, 1993), the model used here can be simplified to yield some analytical results.

In the slab limit, the transit resonance is associated with the dynamics in the parallel direction. However, in the toroidal limit the magnetic curvature and grad-B drifts

cause ions to move in the azimuthal direction (y-direction). In the region of unfavorable magnetic curvature, the magnetic drift (curvature and grad-B drifts) is in the ion diamagnetic direction and so the magnetic drift resonance only exists for the wave propagating in the ion diamagnetic direction which is the ion branch of the toroidal ITG mode. In this toroidal ITG mode calculation, only the magnetic drift resonance is included while the transit resonance is neglected by assuming $k_{\parallel} = 0$.

4.1. The mode with dissipative trapped electrons

In the toroidal limit with $k_{\parallel} = 0$, the perturbed ion density can be written as

$$n_i = n\frac{e\phi}{T_e}\left[-\tau_{\perp} + \left\langle \frac{\omega\tau_{\perp} - \omega_{*i}\left[1+\eta_{i\perp}(u/2-1)+\eta_{i\parallel}(p^2-1/2)\right]}{\omega + i\nu_i - \omega_D(u/2+2\tau_{\perp}p^2/\tau_{\parallel})} \right\rangle \right].$$

By using Eq. (3.2) for the perturbed electron density, the dispersion relation is obtained from the quasi-neutrality condition:

$$D = \frac{\rho_i^2}{k_y^2\lambda_e^2}\left(1 - i\delta + \tau_{\perp} - \left\langle \frac{\omega\tau_{\perp} - \omega_{*i}\left[1+\eta_{i\perp}(u/2-1)+\eta_{i\parallel}(p^2-1/2)\right]}{\omega + i\nu_i - \omega_D(u/2+2\tau_{\perp}p^2/\tau_{\parallel})} \right\rangle \right) = 0 \cdots (4.1)$$

This dispersion relation has been solved numerically for marginal stability and the results will be compared with those of several approximate analytical solutions.

First consider a case without ion collisions ($\nu_i = 0$). By using the approximation of constant energy resonance (CER) (ROMANELLI *et al.*, 1990) $u/2 + 2\tau_{\perp}p^2/\tau_{\parallel} \rightarrow 4(u/2 + p^2)/3$ and setting $b = 0$ in $J_0^2(\langle bu \rangle^{1/2})$, an analytical form of the above dispersion relation is obtained as

$$\frac{1}{\tau_\perp} - i\frac{\delta}{\tau_\perp} + 1 + \frac{3}{2\epsilon_n}\left(-1 + \frac{\eta_{i\parallel}}{3} + \frac{2\eta_{i\perp}}{3}\right) + 2\Omega\left[1 - \frac{3}{2\epsilon_n}\left(\frac{\eta_{i\parallel}}{6} + \frac{\eta_{i\perp}}{3}\right)\right]$$

$$-\sqrt{\Omega}Z(-\sqrt{\Omega})\left\{2\Omega\left[1 - \frac{3}{2\epsilon_n}\left(\frac{\eta_{i\parallel}}{6} + \frac{\eta_{i\perp}}{3}\right)\right] + \frac{3}{2\epsilon_n}\left(-1 + \frac{\eta_{i\parallel}}{2} + \eta_{i\perp}\right)\right\} = 0 \quad \cdots(4.2)$$

with $\Omega = 3\omega/4\omega_D$. From this equation, the resonant mode ($\Omega > 0$) is very different from the non-resonant mode ($\Omega < 0$). For the case $\Omega < 0$, there is no resonance and only electron collisions contribute to the energy exchange between ions and the wave. These two modes are discussed separately below.

For the mode propagating in the ion diamagnetic direction ($\Omega > 0$), the marginal stability boundary can be obtained by solving Eq.(4.1), i.e.,

$$\eta_{i\parallel} = -2\eta_{i\perp} + 4\epsilon_n\left(1 + \frac{1}{\tau_\perp}\right) + \frac{4\epsilon_n\delta}{\tau_\perp Z_i(-\sqrt{\Omega})}\left(Z_r(-\sqrt{\Omega}) - \frac{1}{\sqrt{\Omega}}\right) \quad \cdots(4.3)$$

with the equation for the mode frequency

$$\Omega = \frac{-3\tau_\perp/2\epsilon_n + 3(1+\tau_\perp) + [3Z_r(-\sqrt{\Omega}) - 2/\sqrt{\Omega}]\,\delta/Z_i(-\sqrt{\Omega})}{2 + 2\delta\left[Z_r(-\sqrt{\Omega}) - 1/\sqrt{\Omega}\right]/Z_i(-\sqrt{\Omega})}$$

In the limit $\varepsilon^{1/2}$(i.e., δ) = 0 and $\eta_{i\parallel} = \eta_{i\perp} = \eta_i$, this threshold value of η_i is identical to the one in reference (ROMANELLI *et al.*, 1990). Unlike the slab ITG mode, the marginal stability boundary is now also a function of $\eta_{i\perp}$ for b=0 because the magnetic drift resonance also depends on the perpendicular ion temperature. With the trapped electrons $\varepsilon^{1/2} > 0$, the above result shows that, similar to the slab case, electron collisions can significantly increase the threshold value of the parallel temperature gradient. However, the increase in $\eta_{i\parallel}$ due to electron collisions is not strongly dependent on $\eta_{i\perp}$. An example for $\varepsilon_n = 0.4$ is shown in Fig 4.1(a). To examine the

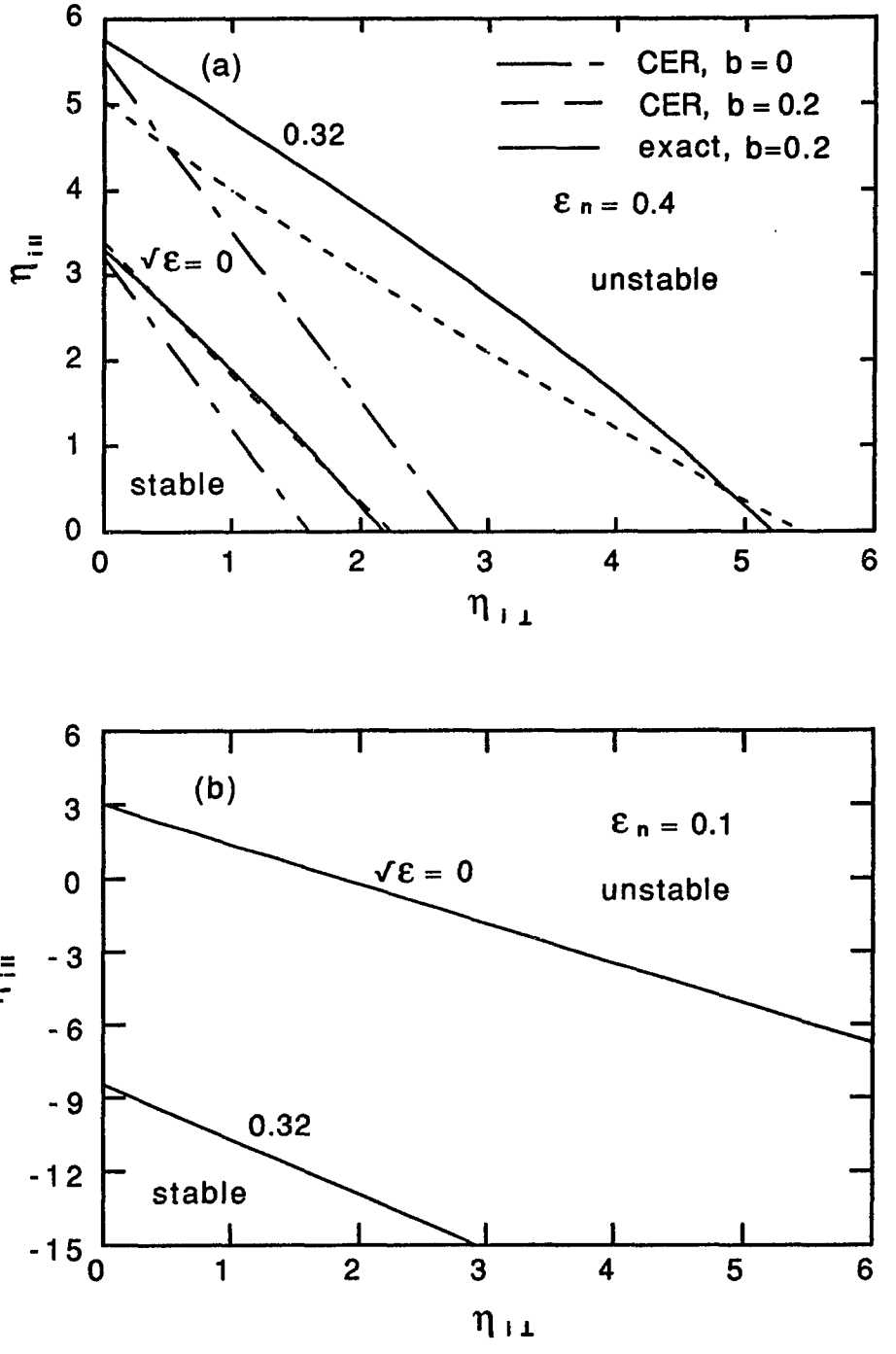

Fig. 4.1 The toroidal branches with electron collisions $\nu_{*e} = 0.1$ when $\tau_I = \tau_\perp = 1$, $\varepsilon^{1/2} = 0$ and 0.32 (a) for the ion branch at large $\varepsilon_n = 0.4$ and (b) for the electron branch at small $\varepsilon_n = 0.1$.

consequences of using the CER approximation and omitting the FLR effect, the CER result with b = 0.2 and the exact results from Eq. (4.1) are also given in Fig. 4.1(a). It shows that the analytical result is fairly good. Note that the resonance condition $\Omega > 0$ poses a constrain on ε_n. When $\varepsilon^{1/2} = 0$, the resonance condition requires $\varepsilon_n > \tau_\perp/2(1 + \tau_\perp)$.

The mode propagating in the electron diamagnetic direction can be obtained at small ε_n, for example, $\varepsilon_n < \tau_\perp/2(1 + \tau_\perp)$ for $\varepsilon^{1/2} = 0$. Because $\Omega < 0$, the integration in Eq. (4.1) yields a real result for $\varepsilon^{1/2} = 0$. Since the dispersion relation only gives one real equation, another equation $\partial D/\partial\Omega = 0$ is used to get the marginal stability boundary for the electron branch (Kim *et al.*, 1992). We confirm Kim's calculation (Kim *et al.*, 1992) by obtaining the solution of Eq. (4.1) numerically for $\varepsilon_n = 0.1$ and b = 0.09. Furthermore, the case is also examined by including electron collisions. The result is shown in Fig. 4.1(b). Contrary to the result for the ion branch, the threshold value of $\eta_{i\|}$ is significantly lowered by electron collisions. It is seen that electron collisions remove the threshold temperature gradient in the positive $\eta_{i\|}$ region. This agrees with the conclusion in the reference (ROMANELLI *et al.*, 1990).

The physics of the ITG instability for the toroidal ion and electron branches is completely different. For the ion branch, the instability arises because there is energy exchange between the resonant ions and the wave. For the electron branch, the magnetic drift resonance no longer exists and the mode is driven unstable by an interchange effect due to the bad magnetic curvature.

The effect of ion collisions has also been considered. Shown in Fig. 4.2 are the results of marginal stability boundary for both the resonant ion branch at large ε_n and the non-resonant electron branch at small ε_n. These results show that, similar to the slab

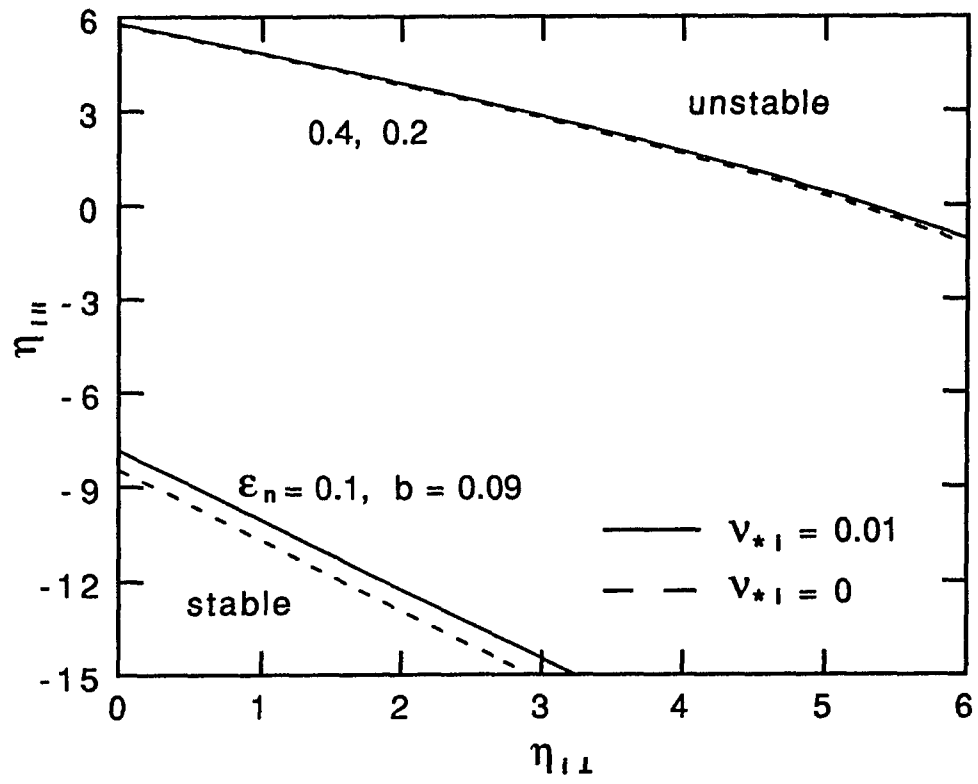

Fig. 4.2 The toroidal branches with ion and electron collisions (ν_{*_i} = 0.01 and ν_{*_e} = 0.10).

case, the threshold is slightly increased and ion collisions have only a weak stabilizing effect.

4.2. The mode with trapped ions

So far the trapped ion response has been neglected based on the frequency ordering that the ion bounce frequency is lower than the mode frequency. However, for low frequency modes, this ordering may no longer be valid. In this section, the trapped

ion response is included under the following frequency ordering:

$$\omega_{te}, \omega_{be} > \nu_{eff,e} \gg |\omega|$$

$$\omega_{ti} \gg \omega_{bi} > |\omega| \gg \nu_{eff,i}.$$

Under this frequency ordering, the trapped ion instability (KADOMTSEV *et al.*, 1971) may be excited. Rosenbluth (ROSENBLUTH *et al.*, 1971) showed that this trapped ion mode can be further destabilized by an ion temperature gradient. For $\eta_i >$ 2/3 the ion Landau damping term for the untrapped ions changes sign and becomes destabilizing, while for $\eta_i > 1.75$ the ion collisional damping term also changes sign. However, this mode propagates in the electron diamagnetic drift direction. Tagger (TAGGER *et al.*, 1977) and Tang (TANG *et al.*, 1977) found that for $\eta_i >$2/3, a new branch of the trapped ion instability arose both in the collisional and collisionless regimes due to a resonance with the magnetic drifts of the ions. This resonant mode propagates in the ion rather than the usual electron diamagnetic direction. Its nonlinear behavior (BIGLARI *et al.*, 1988) may lead to significant thermal and particle transport which in turn presumably reduces η_i to its threshold value at marginal stability.

This resonant trapped ion ITG mode is different from the toroidal ITG mode discussed in the previous section. For the toroidal ITG mode, the instability is driven by the ion temperature gradient with non-adiabatic response of the transit ions. However, for the resonant trapped ion ITG mode, only the non-adiabatic trapped ion response is responsible for the instability.

4.2.1 Dispersion relation

The perturbed trapped-ion density in the electrostatic limit can be written as

$$n_i=\sqrt{\epsilon}n\frac{e\phi}{T_e}\left[-\tau_\perp+\left\langle\frac{\omega\tau_\perp-\omega_{*i}\left[1+\eta_{i\perp}(u/2-1)+\eta_{i\parallel}(p^2-1/2)\right]}{\omega+i\nu_i-\omega_D(u/2+2\tau_\perp p^2/\tau_\parallel)}\right\rangle\right].$$

Because of the frequency ordering used, the adiabatic response can be used for transit ions. The electron response is the same as the one in Eq. (3.2). From quasi-neutrality, the dispersion relation is obtained as

$$1-i\delta+\tau_\perp-\sqrt{\epsilon}\left\langle\frac{\omega\tau_\perp-\omega_{*i}\left[1+\eta_{i\perp}(u/2-1)+\eta_{i\parallel}(p^2-1/2)\right]}{\omega+i\nu_i-\omega_D(u/2+2\tau_\perp p^2/\tau_\parallel)}\right\rangle=0.$$

Based on the consideration that the parallel velocity is lower for the trapped ions, a grad-B model ($u/2 + 2\tau_\perp p^2/\tau_\parallel \rightarrow u/2$) is used to neglect the magnetic curvature drift. For simplicity, the FLR effect is also neglected. Under these approximations, the dispersion relation is simplified to

$$1+\tau_\perp-i\delta-\sqrt{\epsilon}\tau_\perp\left[\frac{\eta_{i\perp}}{\epsilon_n}\right.$$

$$\left.+\left(\frac{1}{\epsilon_n}+\frac{\eta_{i\perp}}{\epsilon_n}(\Omega-1)-\Omega+i\frac{\eta_{i\perp}\nu_{eff,i}}{\epsilon_n\omega_D}\right)\right.$$

$$\left.\times\exp(-\Omega-i\nu_{eff,i}/\omega_D)\,E_1(-\Omega-i\nu_{eff,i}/\omega_D)\right]=0 \quad \cdots(4.4)$$

where $\Omega = \omega/\omega_D$ and E_1 is the exponential integral function (GAUTSCHI *et al.*, 1964).

4.2.2. Collisionless trapped ion ITG mode

First, consider the special case with collisionless trapped ions and adiabatic electron response. In this limit (δ = 0 and ν_i = 0), the dispersion relation reduces to

$$D=1+\tau_\perp-\sqrt{\epsilon}\tau_\perp\left[\frac{\eta_{i\perp}}{\epsilon_n}-\left(\Omega-\frac{\Omega\eta_{i\perp}}{\epsilon_n}-\frac{1-\eta_{i\perp}}{\epsilon_n}\right)\exp(-\Omega)\,E_1(-\Omega)\right]=0 \quad \cdots(4.5)$$

In the fluid-ion limit $|\Omega|>>1$, $\exp(-\Omega)\,E_1(-\Omega)$ can be expanded into

$$\exp(-\Omega)\,E_1(-\Omega)=-\frac{1}{\Omega}-\frac{1}{\Omega^2}-\frac{2}{\Omega^3}-\cdots$$

Then, Eq. (4.5) reduces to

$$1+\tau_\perp+\sqrt{\epsilon}\left[-\tau_\perp+\frac{\tau_\perp}{\Omega}\left(\frac{1}{\epsilon_n}-1\right)+\frac{\tau_\perp}{\Omega^2}\left(-2+\frac{1}{\epsilon_n}+\frac{\eta_{i\perp}}{\epsilon_n}\right)\right]=0$$

where terms to second order in $1/\Omega^2$ are kept to include the case of large temperature gradient $\eta_{i\perp}>>1$. The mode frequency can be solved as

$$\omega=\omega_D\frac{\sqrt{\epsilon}(1-1/\epsilon_n)\pm\sqrt{\epsilon(1/\epsilon_n-1)^2-4[(1+\eta_{i\perp})/\epsilon_n-2][\sqrt{\epsilon}(1+1/\tau_\perp)-2\epsilon]}}{2[1+1/\tau_\perp-\sqrt{\epsilon}]}.$$

For very small ε_n, the modes propagate in the electron diamagnetic direction without any damping or growth. As ε_n increases, the mode frequency acquires an imaginary part because the term with $\eta_{i\perp}$ in the square root dominates. When $\varepsilon_n \sim 1$, the mode frequency becomes purely imaginary and the growth rate is given by

$$\gamma\sim-(\epsilon)^{1/4}\omega_D\sqrt{\eta_{i\perp}/\epsilon_n(1+\tau_\perp^{-1})}$$

This is simply the collisionless trapped ion instability (KADOMTSEV *et al.*, 1971) with an ion temperature gradient.By using this result, $|\Omega| \sim \gamma/\omega_D \sim 1$ is obtained with the

experimental parameters $\varepsilon = 0.24$, $\tau_\perp = 0.4$, $\varepsilon_n = 1..6$ and $\eta_{i\perp} = 18$ for the nearly flat density shots in TFTR (ZARNSTORFF *et al.*, 1991). However, now the assumption $|\Omega| >> 1$ is no longer valid. Although the expansion procedure is often used in discussions (XU *et al.*, 1991; BIGLARI *et al.*, 1989), a better way to find the growth rate is to solve the dispersion relation given by Eq. (4.5) numerically. The result is shown in Fig. 4.3. It can be seen that the fluid-ion approximation is only valid for an extremely large $\eta_{i\perp}$. In the experimental range, the mode propagating in the ion diamagnetic direction approaches the magnetic drift frequency while the growth rate becomes almost zero. This is simply the condition for the magnetic drift resonance.

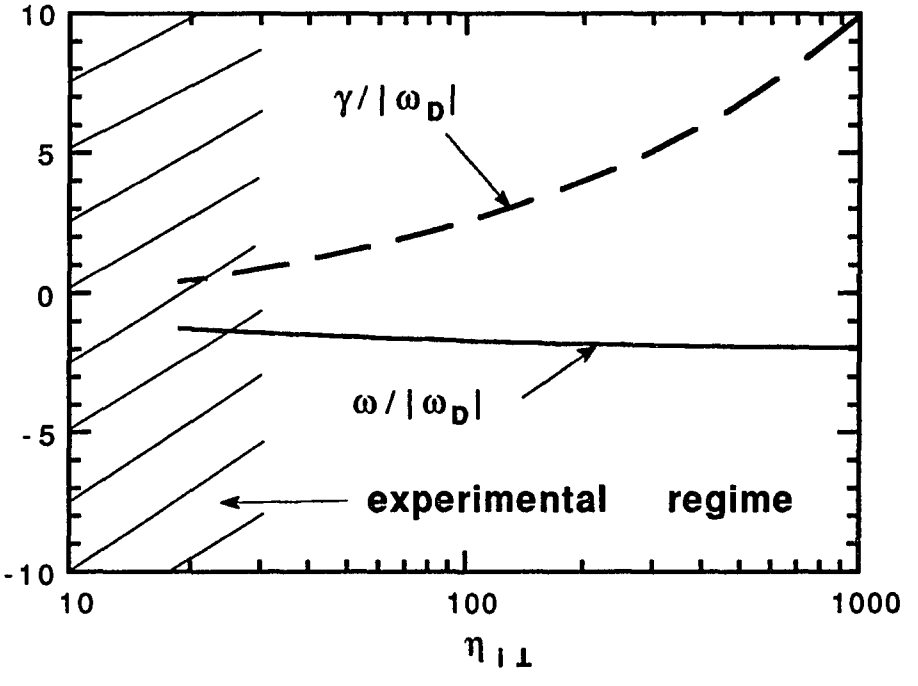

Fig. 4.3 Growth rate and real frequency versus $\eta_{i\perp}$ with $\varepsilon = 0.24$, $\tau_\perp = 0.4$ and $\varepsilon_n = 1.6$.

Thus, in order to explain the experimental results, the magnetic drift resonance must be included in the analysis.

When the magnetic drift resonance is considered, analytical results for marginal stability can be obtained from the dispersion relation given by Eq. (4.5). Note that D is a complex function because $E_1(-\Omega)$ is complex for $\Omega>0$. By setting the imaginary part of D to zero, the marginal frequency is obtained as

$$\omega=\omega_D\frac{\eta_{i\perp}-1}{\eta_{i\perp}-\epsilon_n} \quad \cdots(4.6)$$

The resonant condition of $\Omega>0$ requires $\eta_{i\perp} > 1$. Here $\eta_{i\perp} > \varepsilon_n$ is always true for marginal stability (the proof of this is given later). This necessary condition partially agrees with the results in the reference (TAGGER *et al.*, 1977, TANG *et al.*, 1977). Instead of $\eta_{i\perp} > 2/3$ of the references, $\eta_{i\perp} > 1$ is obtained when the anisotropy in the ion temperature gradient is included.

By setting the real part of D to be zero, the threshold value of $\eta_{i\perp}$ is given by

$$\eta_{i\perp}=\frac{\epsilon_n}{\sqrt{\epsilon}}\left(1+\frac{1}{\tau_\perp}\right) \quad \cdots(4.7)$$

The above results indicate that only the perpendicular ion temperature gradient is crucial. The parallel temperature gradient plays no role because the ion magnetic drift is solely determined by the perpendicular velocity of the ions. This should be contrasted with the toroidal ITG mode discussed in the previous section where both parallel and transverse velocities were taken into account in the magnetic drift. Then, the grad-B model is not a good choice. By using the CER approximation, it is shown that the mode can be driven unstable by either a perpendicular or parallel temperature gradient. The

other feature of the mode is that the threshold value of $\eta_{i\perp}$ is now increased by a factor of $1/\varepsilon^{1/2}$. The reason for this is that the ions participating in the resonance are only the trapped ions with the trapped fraction of $\varepsilon^{1/2}$. Compared with the experimental threshold value $\varepsilon_T^{-1} \sim 11$, where $\varepsilon_T^{-1} \equiv \eta_i/\varepsilon_n$, (ZARNSTORFF *et al.*, 1991), the result from Eq. (4.7) is 7.1 that is better than the one ($\varepsilon_T^{-1} \sim 5$) obtained by using a particle simulation code (XU *et al.*, 1991). It seems that the trapped ion toroidal ITG model gives a better agreement than the toroidal ITG model.

Actually, the threshold temperature gradients given by Eqs. (4.3) and (4.7) are independent of the density gradient for both the collisionless toroidal ITG mode and the trapped ion toroidal ITG mode. This agrees with the experimental observation (ZARNSTORFF *et al.*, 1991) that the threshold temperature gradient was almost constant while the density profiles were broadened significantly. It was suggested (DOMINGUEZ *et al.*, 1988) that the threshold value should not be η_i, as typically quoted. Rather, the stability threshold should be characterized by $\varepsilon_T \equiv \varepsilon_n/\eta_i = L_T/R$ with $L_T = -(d\ln T_i/dx)^{-1}$. Using this definition, the threshold value given by Eq.(4.7) can be rewritten as

$$\epsilon_{T_\perp} = \sqrt{\epsilon}\,\frac{\tau_\perp}{1+\tau_\perp}$$

where $\varepsilon_{T\perp} \equiv \varepsilon_n/\eta_{i\perp}$.

4.2.3. The effect of collisions

In reality, both ion and electron collisions exist. First the effect of trapped electron collisions on the threshold value of the ion temperature gradient is investigated.

With trapped electron collisions, the marginal frequency and the threshold value of $\varepsilon_{T\perp} \equiv \varepsilon_n/\eta_{i\perp}$ can be solved analytically from the dispersion relation given by Eq. (4.4), yielding

$$\omega = \omega_D \left[\frac{\epsilon_n - \epsilon_{T_\perp}}{\epsilon_n (1-\epsilon_{T_\perp})} + \frac{\delta \epsilon_{T_\perp} \exp(\Omega)}{\pi \sqrt{\epsilon} \tau_\perp (1-\epsilon_{T_\perp})} \right]$$

and

$$\epsilon_{T_\perp} = \frac{\sqrt{\epsilon}\tau_\perp}{1+\tau_\perp + \delta E_1(\Omega)/\pi}$$

where E_1 is the exponential integral function (GAUTSCHI *et al.*, 1964). For $\Omega \sim 1$, $E_1(\Omega) > 0$ and electron collisions lower the threshold value of $\varepsilon_{T\perp}$. In other words, a higher threshold value of the perpendicular temperature gradient is needed for instability. To see how electron collisions quantitatively affect the threshold $\varepsilon_{T\perp}$, the parameters $\nu_{eff,e}/\omega_{be} = 0.1$, $L_n/qR \sim 1$, $\eta_e = 0$, $\tau_\perp = 0.4$, $\varepsilon = 0.24$ and $\varepsilon_n = 1.6$ are used to calculate $\varepsilon_{T\perp}$ for TFTR shot (ZARNSTORFF *et al.*, 1991). The value of $\varepsilon_{T\perp}$ is found to increase from 7.1 to 7.7 due to electron collisions.

Secondly, the effects of trapped ion collisions are considered. The collisionality is usually low for ions and so only terms to first order in $\nu_{eff,i}$ are kept. Thus, the analytical expansions for the marginal frequency and the threshold temperature gradient can be obtained as

$$\omega = \omega_D \left[\frac{\epsilon_n - \epsilon_{T_\perp}}{\epsilon_n (1-\epsilon_{T_\perp})} + \frac{(\delta + \sqrt{\epsilon} A_1)\, \epsilon_{T_\perp} \exp(\Omega)}{\pi \sqrt{\epsilon} \tau_\perp (1-\epsilon_{T_\perp})} \right] \quad \cdots (4.8)$$

and

$$\epsilon_{T_\perp} = \frac{\pi\sqrt{\epsilon}\tau_\perp}{\pi\,(1+\tau_\perp-\sqrt{\epsilon}A_2)+\delta E_i(\Omega)}$$

where

$$A_1 = \frac{\tau_\perp \nu_{eff,i}}{\omega_D}\left\{\left(\frac{1}{\Omega}-\exp(-\Omega)\,E_i(\Omega)\right)\times\left[\Omega\left(1-\frac{1}{\epsilon_{T_\perp}}\right)-\frac{1}{\epsilon_n}+\frac{2}{\epsilon_{T_\perp}}\right]-\frac{1}{\epsilon_{T_\perp}\Omega}\right\}$$

and

$$A_2 = \frac{\pi\tau_\perp \nu_{eff,i}}{\omega_D}\left[\Omega\,(1-\frac{1}{\epsilon_{T_\perp}})-\frac{1}{\epsilon_n}+\frac{2}{\epsilon_{T_\perp}}\right]\exp(-\Omega)$$

The major correction to the threshold $\varepsilon_{T\perp}$ is from A_2. Since $A_2>0$, ion collisions also lower the threshold value of $\varepsilon_{T\perp}$. Using $\nu_{eff,i}/\omega_{bi} = 0.01$, it is found that $\varepsilon_{T\perp}^{-1}$ increases from 7.7 to 8.3. This shows that ion collisions further stabilize the mode.

Both electron and ion collisions have stabilizing effects on the resonant trapped ion instability but the correction to the threshold value of $\varepsilon_{T\perp}$ is quite modest. The reason is that the strong magnetic drift resonance dominates the exchange of energy between the waves and the ions. There are only two ways in which the exchange of energy can occur: one is due to the magnetic drift resonance and the other is due to collisions.

Figure 4.4 is used to explain the trapped ion toroidal ITG instability. The power transferred from the ions to the waves due to the magnetic drift resonance can be expressed as

$$P = -\int d\vec{v}\; eE_y v_D\left[F\left(x+\frac{E_y C}{B}\delta t, v_\perp+\delta v_\perp\right)-F\left(x-\frac{E_y C}{B}\delta t, v_\perp-\delta v_\perp\right)\right]$$

where $\delta v_\perp$ is the change in velocity in a time interval δt owing to the $\mathbf{E}\times\mathbf{B}$ drift in the

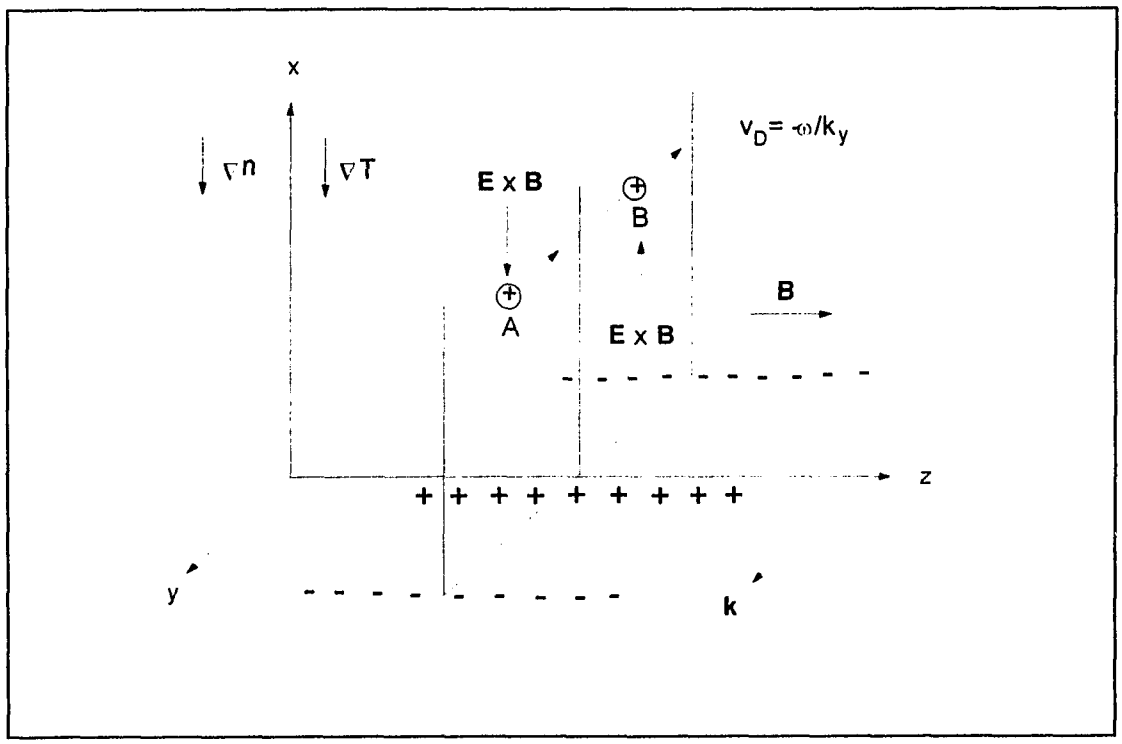

Fig. 4.4 The trapped ion toroidal ITG instability

x-direction. $\delta v_\perp = -v_\perp(\delta t E_y c/B)/2R$ because of invariance of the magnetic moment. After integrating over the velocity space, P reduces to

$$P=\frac{2\sqrt{\epsilon}neE_y^2 v_D v_\perp c\delta t}{Bv_{\perp 0}^2 L_n}\Delta v_\perp\left[1+\eta_i\left(\frac{v_\perp^2}{2v_{\perp 0}^2}-1\right)-\epsilon_n\frac{v_\perp^2}{2v_{\perp 0}^2}\right]\exp\left(-\frac{v_\perp^2}{2v_{\perp 0}^2}\right)\Bigg|_{v_\perp=\sqrt{2R\omega_c v_D}} \quad \cdots(4.9)$$

where $\Delta v_\perp$ is the perpendicular velocity range corresponding to the resonant velocity. $\Delta v_\perp = R\omega_c \Delta v_D/v_\perp$, because $v_D = v_\perp^2/2R\omega_c$. The range of v_D for the resonant ions is approximately within $\Delta v_D \sim (\pi/4k_y)\delta t$. For the resonant ions $v_D = -\omega/k$. Substituting

$\Delta v_{\perp}$ and v_D into Eq. (4.9), the power density transferred to the wave can be written as

$$P=-\frac{\sqrt{\epsilon}\pi e^2 n_0 E_y^2 \omega v_{ith} \rho_i^2}{2k_y^2 T_\perp L_n}\left(\frac{1}{\epsilon_n}+\frac{1}{\epsilon_{T_\perp}}(\Omega-1)-\Omega\right)\exp(-\Omega)$$

The first term is related to the density gradient. It is positive (ω <0 here) and so power is transferred to the wave. The second and third terms come from the perpendicular temperature gradient. The last term is the contribution from the variation of the magnetic field. This term is negative and so power is transmitted to resonant ions.

The power transferred to the wave due to electron and ion collisions is given by

$$P'=\omega(\delta+\sqrt{\epsilon}A_1)\frac{\rho_i^2 v_{ith} E_y^2}{8\pi k_y^2 L_n \lambda_e^2}$$

Here, the power is always transferred to resonance ions. Because the total wave energy is positive for the toroidal ITG mode ($k_\parallel$ = 0), the mode is now stabilized by the dissipation from collisions. For marginal stability, there is no net energy transfer between the wave and the resonant ions and so these two powers must balance each other. It is easy to prove that the balance condition P+P' = 0 gives the marginal frequency given by Eq. (4.8). Here we see that the power transfer due to the resonance exponentially decreases with increasing Ω. From Fig. (4.3), it can be seen that the TFTR shot corresponds to the case $\Omega \sim 1$. Therefore, the resonant part is dominant and collisions have only a modest effect on the mode. However, if $\Omega >> 1$, the resonance becomes so weak that the power due to collisions can become dominant. In this case, both electron and ion collisions may play important roles.

4.3. Conclusion

In the toroidal case, both the parallel temperature gradient $\eta_{i\parallel}/\varepsilon_n$ and perpendicular temperature gradient $\eta_{i\perp}/\varepsilon_n$ are needed to trigger the ITG instability. For small ε_n, an electron branch can become unstable. There is no magnetic drift resonance. The mode is driven unstable by the interchange effect. Collisions from the dissipative trapped electrons can further destabilize the mode. For large ε_n, an ion branch is found to be unstable. This branch is driven unstable by the coupling between the magnetic drift and ion temperature gradient. Collisions from the dissipative trapped electrons have a stabilizing effect on the mode. For the resonant trapped ion ITG instability, only $\eta_{i\perp}/\varepsilon_n$ is needed to trigger the instability. The threshold $\eta_{i\perp}/\varepsilon_n$ for the resonant mode is increased by a factor of $1/\varepsilon^{1/2}$ because only the trapped ions participate in the resonance. Electron and ion collisions can further stabilize the mode.

CHAPTER 5

MIXED SLAB AND TOROIDAL ITG MODES

As discussed in the previous chapters, the slab and toroidal ITG modes are driven unstable by the interaction between the wave and the resonant ions. For the slab case, the transit resonance occurs when the parallel ion velocity matches the phase velocity of the mode. For the toroidal mode, the magnetic drift resonance happens when the magnetic drift velocity in the transverse direction is equal to the phase velocity of the mode. In general, the velocity of the ion guiding center can have both parallel or perpendicular components and so the transit and the magnetic drift resonances can exist simultaneously. Now, the condition for resonance becomes $\omega = \mathbf{k}\cdot\mathbf{v} = k_{\parallel}v_{\parallel} + k_y v_D$. This more realistic case is investigated in this chapter.

The mixed slab and toroidal ITG mode is first discussed for both collisionless and collisional cases. Then, a model with trapped ions is studied and its results are applied to the Columbia Linear Machine (CLM).

5.1. With dissipative trapped electrons

5.1.1. Dispersion relation

The perturbed ion density with both transit and magnetic drift resonances is

$$\frac{n_i}{n_0}=\frac{e\phi}{T_e}\left(-\tau_\perp+\left\langle\frac{\tau_\perp\omega+(\tau_\parallel-\tau_\perp)\,k_\parallel p-\omega_{*i}\,(1-\eta_{i\perp}-\eta_{i\parallel}/2+p^2\eta_{i\parallel}+\eta_{i\perp}u/2)}{\omega+i\nu_i-k_\parallel p-\omega_D(u/2+2\tau_\perp p^2/\tau_\parallel)}\right\rangle\right).$$

From quasi-neutrality $n_i = n_e$, with the perturbed electron density given by Eq. (3.2), the dispersion relation is obtained as

$$1-i\delta+\tau_\perp-\left\langle\frac{\tau_\perp\omega+(\tau_\parallel-\tau_\perp)\,k_\parallel p-\omega_{*i}\,(1-\eta_{i\perp}-\eta_{i\parallel}/2+p^2\eta_{i\parallel}+\eta_{i\perp}u/2)}{\omega+i\nu_i-k_\parallel p-\omega_D(u/2+2\tau_\perp p^2/\tau_\parallel)}\right\rangle=0 \quad \cdots(5.1)$$

An analytical expression of the above dispersion relation can be obtained by using the CER approximation and expanding $J_0^2((bu)^{1/2})$ to first order in b. After some manipulations relegated to Appendix A, the dispersion relation reduces to

$$1-i\delta+\tau_\parallel-b(\tau_\parallel-\tau_\perp)+\left\{F\left[-\tau_\parallel\frac{\omega}{k_\parallel}+i\frac{\nu_i}{k_\parallel}(\tau_\perp-\tau_\parallel)+\frac{\omega_{*i}}{k_\parallel}\left(1-\eta_{i\perp}-\frac{\eta_{i\parallel}}{2}\right)\right]\right.$$

$$+\left(\frac{\partial F}{\partial\beta}+\frac{16\omega_D^2}{9k_\parallel^2}\frac{\partial^2F}{\partial\alpha^2}\right)\left(\frac{4\omega_D}{3k_\parallel}(\tau_\perp-\tau_\parallel)+\frac{\omega_{*i}\eta_{i\perp}}{k_\parallel}\right)$$

$$\left.+\left(\frac{\partial F}{\partial\alpha}-\frac{16\omega_D^2}{9k_\parallel^2}\frac{\partial^2F}{\partial\alpha^2}-\frac{9k_\parallel^2}{64\omega_D^2}F\right)\left(\frac{\omega_D}{k_\parallel}(\tau_\perp-\tau_\parallel)+\frac{\omega_{*i}\eta_{i\parallel}}{k_\parallel}\right)\right\}\Bigg|_{\alpha,\beta=1}=0 \quad \cdots(5.2)$$

where

$$F=F_0+b\left[\frac{\partial F_0}{\partial\beta}+\left(\frac{4\omega_D}{3k_\parallel}\right)^2\frac{\partial^2F_0}{\partial\alpha^2}\right],$$

$$F_0=\frac{1}{\alpha}[Z(A+B)-Z(A-B)]\exp\left(\frac{-9k_\parallel^2(1-\alpha^2/\beta)}{64\omega_D^2}\right),$$

with

$$A=-\left(\frac{3\beta(\omega+iv_i)}{4\omega_D}+\frac{9\beta k_\parallel^2}{64\omega_D^2}\right)^{1/2}$$

$$B=\frac{3\alpha k_\parallel}{8\sqrt{\beta}\omega_D}.$$

Equation (5.2) thus describes the case of the mixed mode with electron and ion collisions.

5.1.2. Marginal stability boundaries without collisions

Before considering the effects of collisions, we first discuss the effect of coupling between the electron and ion branches of the mode when both the magnetic drift and transit resonances are present. This effect becomes important when we raise ε_n with a finite $k_\parallel$. As discussed in the slab limit in Chapter 3, the upper boundary (ion branch) and the lower boundary (electron branch) are separated in the $\eta_\parallel$-$\eta_\perp$ plane. However, with an increase in ε_n, the two boundaries approach each other. When they meet, the coupling between the upper and lower boundaries causes a split in the stability region. This effect is shown in Fig. 5.1(a) and 5.1(b) with $k_\parallel = 0.1$ and ε_n increasing from 0.04

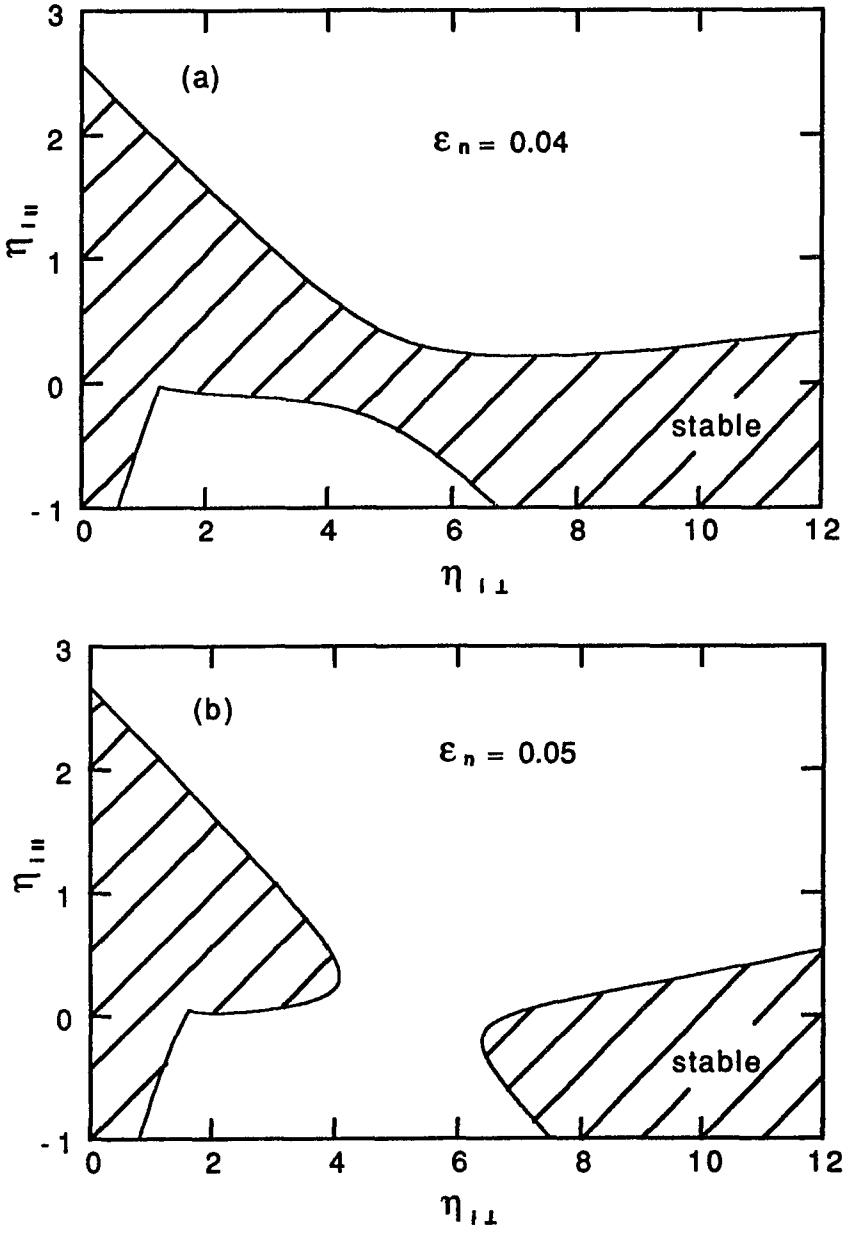

Fig. 5.1 The marginal stability diagram in the $\eta_{i\parallel}$-$\eta_{i\perp}$ plane for a mixed slab and toroidal case with a CER approximation when $\tau_i = \tau_\perp = 1$, b=0.2 and $k_\parallel L_n = 0.1$. (a) $\varepsilon_n = 0.04$ and (b) $\varepsilon_n = 0.05$.

to 0.05. The threshold temperature gradients are obtained from the analytical expression, Eq. (5.2). Note that the split occurs for small ε_n. This enables us to examine this effect analytically by expanding the dispersion relation to first order in ε_n. The threshold $\eta_{i\parallel}$ is then given by

$$\eta_{i\parallel} = 1 - \eta_{i\perp} bG - C_1 \epsilon_n$$

$$\pm \left[(1 - \eta_{i\perp} bG - C_1 \epsilon_n)^2 + \frac{2k_\parallel^2}{\omega_{*i}^2} \left(\tau_\parallel - \tau_\perp + \frac{1+\tau_\perp}{S_0} \right) \left(-\tau_\perp + \frac{1+\tau_\perp}{S_0} \right) - C_2 \epsilon_n \right]^{1/2} \quad \cdots (5.3)$$

where $C_1 \sim b(\eta_{i\perp} k_y / k_\parallel)^2$ and $C_2 \sim 10 \eta_{i\perp} k_y^2 / k_\parallel$ for large $\eta_{i\perp}$. Here the square root term represents the distance between the upper and lower boundaries. For $\varepsilon_n = 0$, the terms in the square root are always positive. However, for $\varepsilon_n > 0$, the negative contribution from the C_2 term can reduce the distance. Here, the stability region becomes smaller due to an increase in the destabilizing effect of the grad-B and curvature drifts. Note that the distance depends on $\eta_{i\perp}$. The split occurs when the minimum distance is reduced to zero. From this condition the minimum ε_n needed for the split can be estimated to be: $\varepsilon_n \sim (k_\parallel / k_y)^2$.

The lower boundaries in Fig. 5.1(a) and 5.1(b) appear not to be smooth. The point of discontinuity corresponds to a change from the resonant to the non-resonant mode. In the slab case, the condition for transit resonance can always be satisfied. In the toroidal case, only the wave propagating in the ion diamagnetic direction can satisfy the condition of the magnetic drift resonance. For the mixed slab and toroidal mode, both the transit and magnetic drift resonances occur if the denominator of Eq. (5.1)

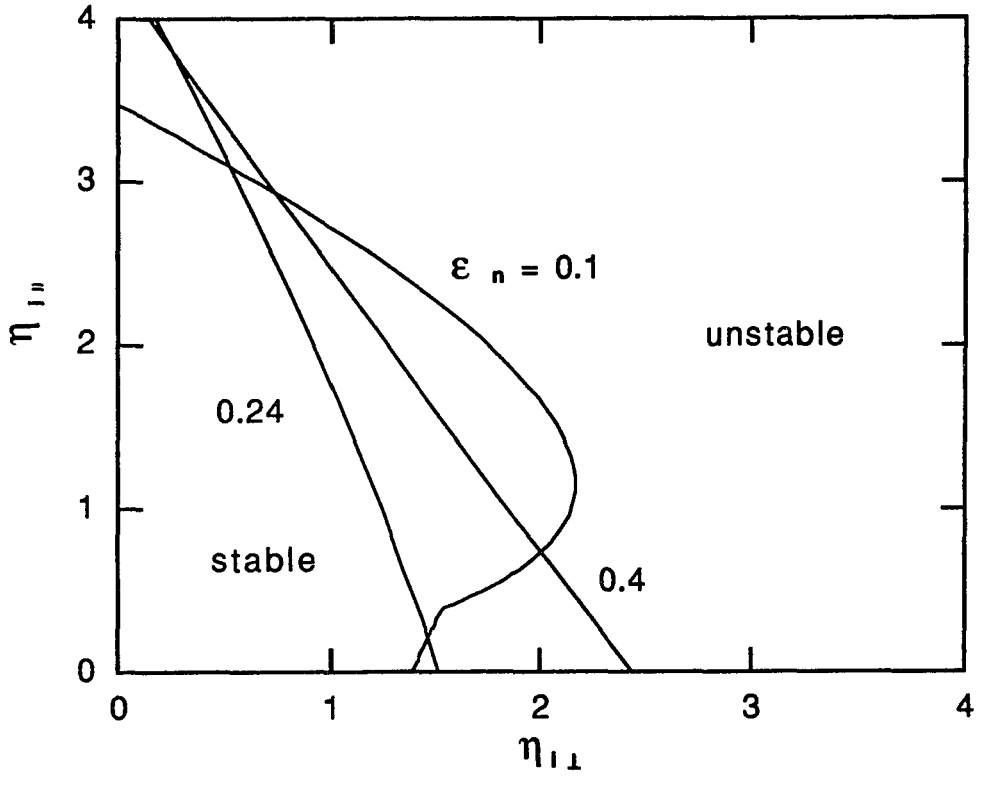

Fig. 5.2 The marginal stability diagram at small $\eta_{i\perp}$ for a mixed slab and toroidal case with a CER approximation when $\tau_\parallel = \tau_\perp = 1$, b=0.2 and $k_\parallel L_n = 0.1$.

is equal to zero for an appropriate ω. This gives a resonant condition $\omega < k_\parallel^2(\tau_\parallel\tau_\perp/2)^{1/2}/4\varepsilon_n$, which is always satisfied for the ion branch. The resonances still exist for the electron branch for this condition. However, when $\omega > k_\parallel^2(\tau_\parallel\tau_\perp/2)^{1/2}/4\varepsilon_n$, there is no resonance for the electron branch. In this situation, the condition $\partial D/\partial\omega = 0$ is used to get the marginal stability boundary.

The split of the stability region creates two new stability regions in the $\eta_{i\parallel}$-$\eta_{i\perp}$ plane: one at small $\eta_{i\perp}$ and the other at large $\eta_{i\perp}$. Figure 5.2 shows how the stability

region at small η_i, changes as ε_n is further increased. As we expect, the results approach the toroidal ones with an increase in ε_n. The threshold $\eta_i = \eta_{i\parallel} = \eta_{i\perp}$ reaches a minimum at $\varepsilon_n \sim 0.2$ for the case of isotropic η_i. This agrees well with the results of reference (ROMANELLI *et al.*, 1989). The stability boundary at large $\eta_{i\perp}$, shown in Fig. 5.1, can appear in the positive $\eta_{i\parallel}$ region. This result is not accurate because the approximations of CER and small b were used to obtain Eq. (5.2). To see how these approximations affect the analytic result, the dispersion relation is solved without any approximation by a numerical approach. The result is shown in Fig. 5.3 and Fig. 5.4. The basic features of the marginal stability boundary from the analytical expression are evident. However, the stability region at large $\eta_{i\perp}$ is now in the negative region of $\eta_{i\parallel}$. Since positive $\eta_{i\parallel}$ is usually found in experiments, the new stability region at large $\eta_{i\perp}$ is not important practically.

5.1.3. Marginal stability boundaries with collisions

With collisions, the coupling effect plays an even more important role when both ε_n and $k_\parallel$ are considered. It has been shown in Chapter 3 that in the slab limit, the upper and lower boundaries change significantly with collisions. Because of the coupling between these two branches, the new marginal stability boundaries become quite different from the ones without collisions.

First, examine this coupling effect analytically. With collisions, the threshold $\eta_{i\parallel}$ from Eq. (5.3) becomes

$$\eta_{i\parallel} = 1 - \eta_{i\perp} bG - C_1 \epsilon_n + \frac{k_\parallel \delta}{\omega_{*i} S_0 Z_i}$$

$$\pm\left[\left(1-\eta_{i\perp}bG-C_1\epsilon_n+\frac{k_\parallel\delta}{\omega_{*i}S_0Z_i}\right)^2-C_2\epsilon_n+\frac{2k_\parallel^2}{\omega_{*i}^2}\left(\tau_\parallel-\tau_\perp+\frac{1+\tau_\perp}{S_0}\right)\left(-\tau_\perp+\frac{1+\tau_\perp}{S_0}\right)\right.$$

$$\left.+\frac{2k_\parallel^2Z_r\delta}{\omega_{*i}^2S_0Z_i}\left(\tau_\parallel-2\tau_\perp+\frac{2+2\tau_\perp}{S_0}-\frac{Z_r\delta}{Z_iS_0}\right)\right]^{1/2}$$

Here the collisional contributions can cancel the term with C_2 and diminish the coupling effect. Using the same procedure as in the previous section, the change in the minimum ε_n needed for the coupling is $\Delta\varepsilon_n \sim (k_\parallel/k_y)^2Z_r\delta/Z_i > 0$ at the coupling point. This means that a larger ε_n is needed for significant coupling to occur.

The exact solution for the marginal stability boundary with both electron and ion collisions is shown in Fig. 5.5(a) and 5.5 (b). Compared with the collisionless results in Fig. 5.3(a) and 5.3(b), two new features are apparent. First, the stability region at small $\eta_{i\perp}$ is dramatically reduced because the electron branch is destabilized by electron collisions. As discussed before, this effect depends on the FLR effect. Secondly, the new stability boundary at large $\eta_{i\perp}$ appears in the positive $\eta_{i\parallel}$ region. The wave corresponding to this branch propagates in the ion diamagnetic direction for positive $\eta_{i\parallel}$. Therefore, another stability region is found for the mixed slab and toroidal case. Another way to understand these results is to compare them with the slab results in Fig. 3.3. The destabilizing effect of the grad-B drift causes a coupling between the lower and upper boundaries, which breaks the stability region into two: one at small $\eta_{i\perp}$ and the other at large $\eta_{i\perp}$.

The stability boundaries at small $\eta_{i\perp}$ for large ε_n are shown in Fig. 5.6. Compared with the collisionless results with an isotropic ion temperature gradient, the threshold η_i is increased about 20% for $\varepsilon_n = 0.24$. Due to electron collisions, a

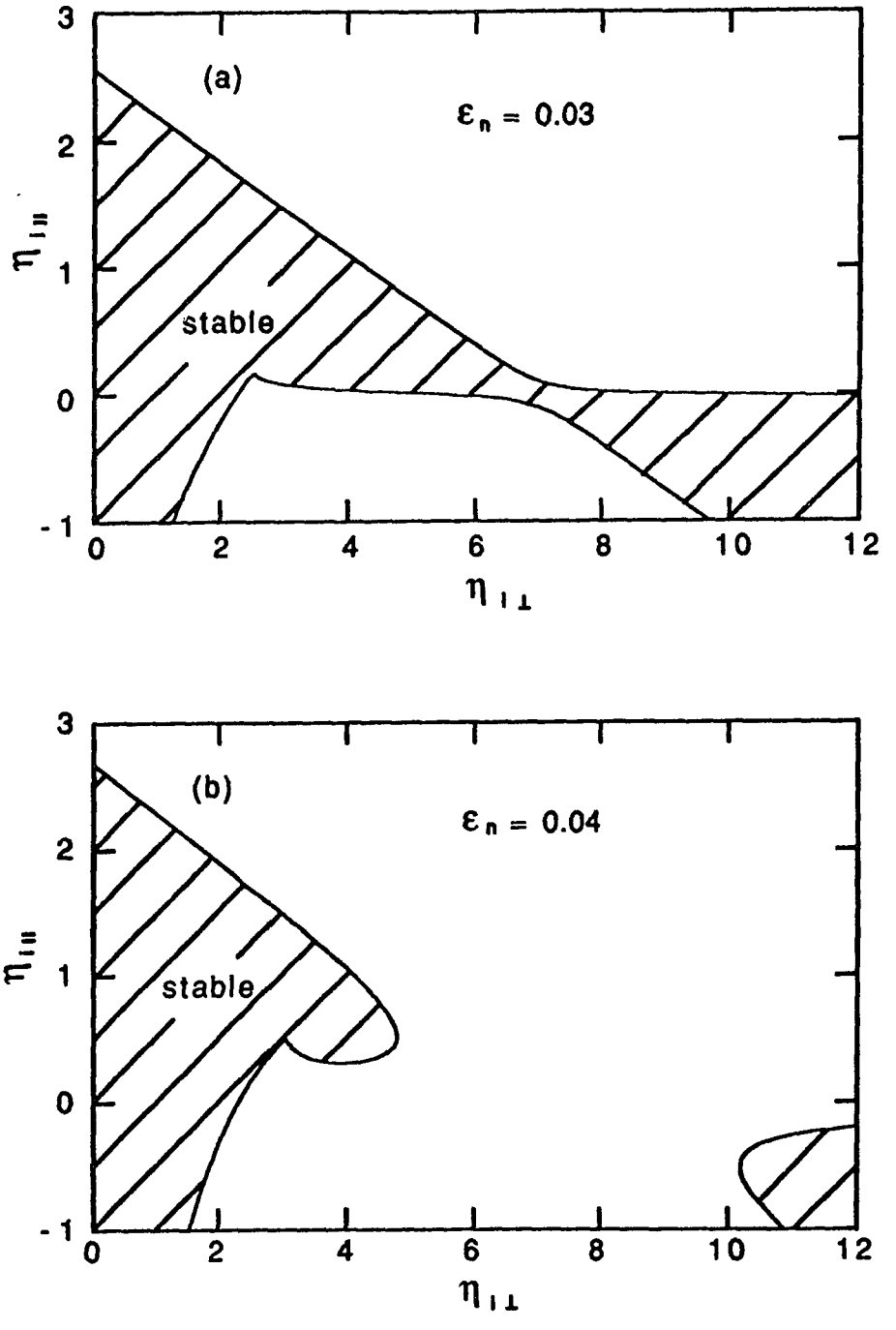

Fig. 5.3 The marginal stability diagram in the $\eta_{i\parallel}$-$\eta_{i\perp}$ plane for a mixed slab and toroidal case from an exact solution of Eq. (5.1) when $\tau_i = \tau_\perp = 1$, b=0.2 and $k_\parallel L_n$ = 0.1. (a) ε_n = 0.04 and (b) ε_n = 0.05.

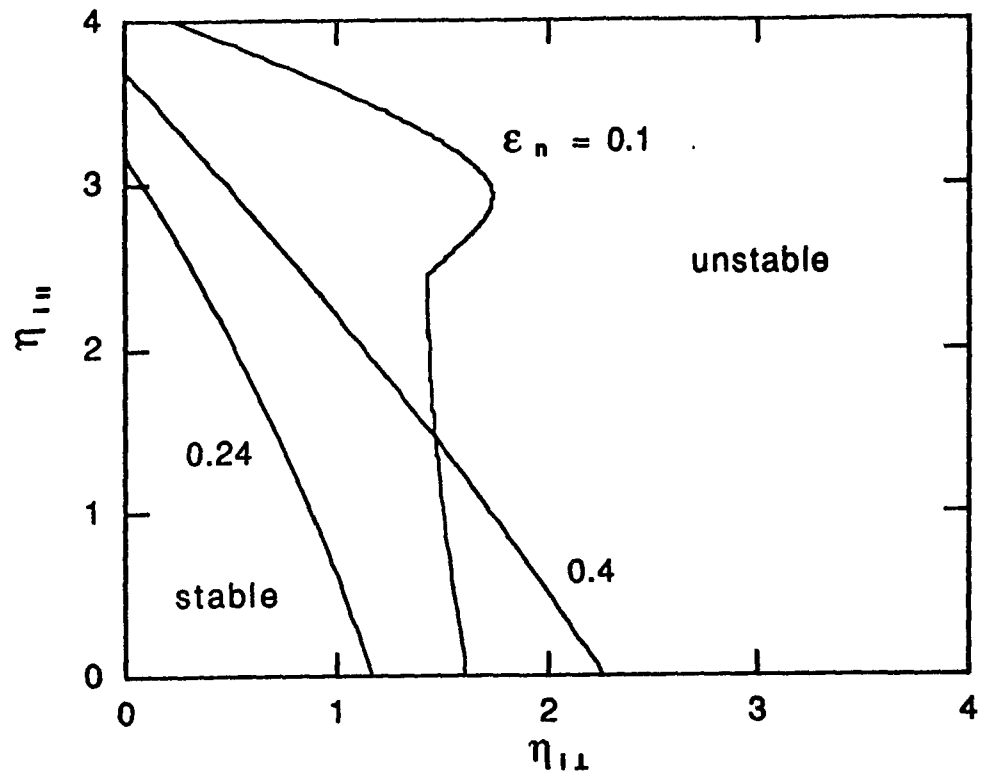

Fig. 5.4 The marginal stability diagram at small $\eta_{i\perp}$ for a mixed slab and toroidal case with an exact solution to Eq. (5.1) when $\tau_i = \tau_\perp = 1$, b=0.2 and $k_\parallel L_n = 0.1$.

minimum threshold appears at $\eta_i \sim 0.7$ in the isotropic case. Below this value, an unstable electron branch can be generated. This result agrees with reference (ROMANELLI *et al.*, 1989).

The new stability region at large $\eta_{i\perp}$ forms a second stability regime which was not found in previous work (KIM J.Y. *et al.*, 1992, ROMANELLI *et al.*, 1989). Because the threshold $\eta_{i\parallel}$ is positive, the stability regime is important on practical grounds.

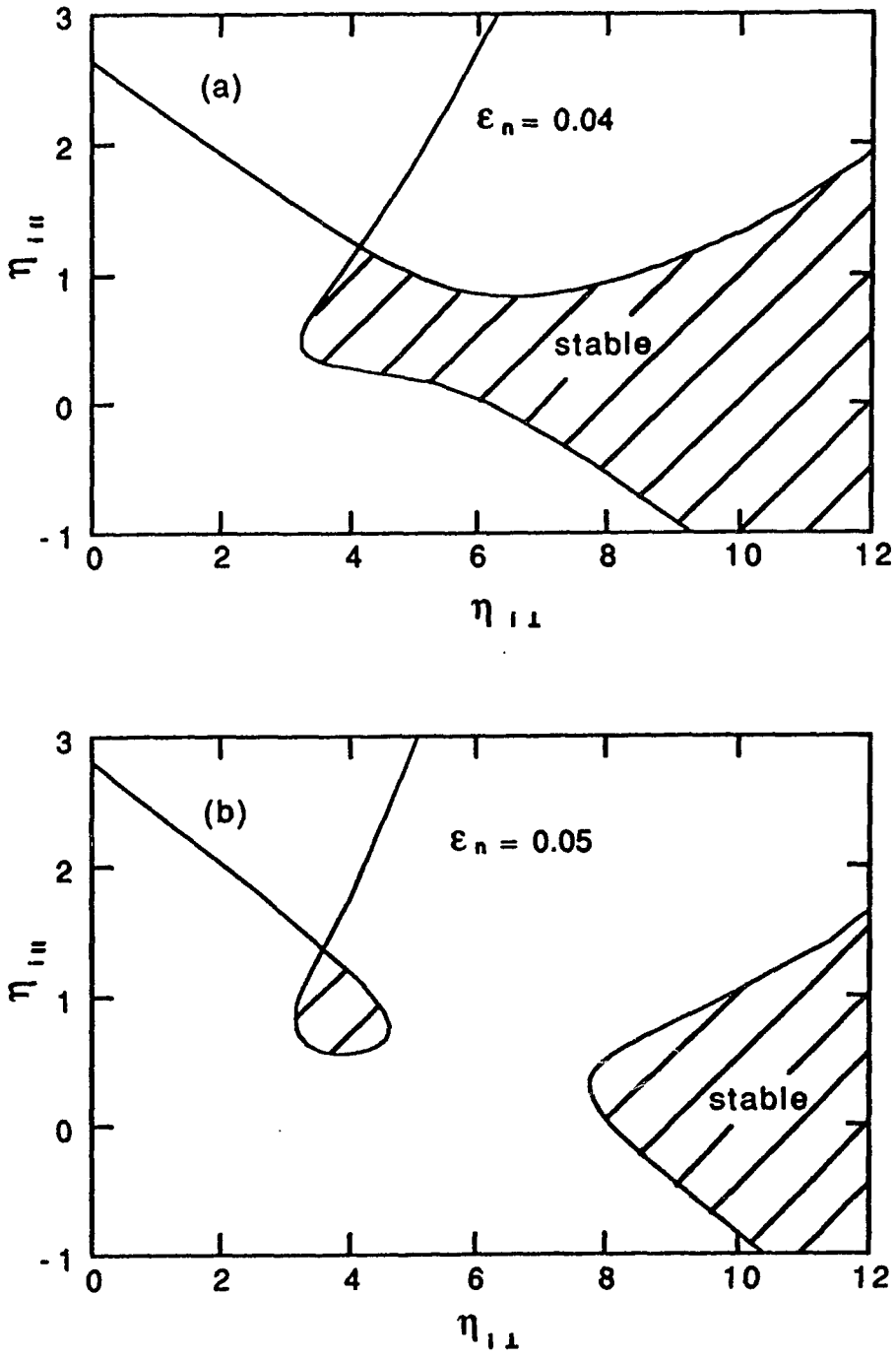

Fig. 5.5 The marginal stability diagram in the $\eta_{i\parallel}$-$\eta_{i\perp}$ plane for a mixed slab and toroidal case with both electron and ion collisions ($\nu_{*i} = 0.01$ and $\nu_{*e} = 0.1$) when $\tau_i = \tau_\perp = 1$, b=0.2 and $k_\parallel L_n = 0.1$. (a) $\varepsilon_n = 0.04$ and (b) $\varepsilon_n = 0.05$.

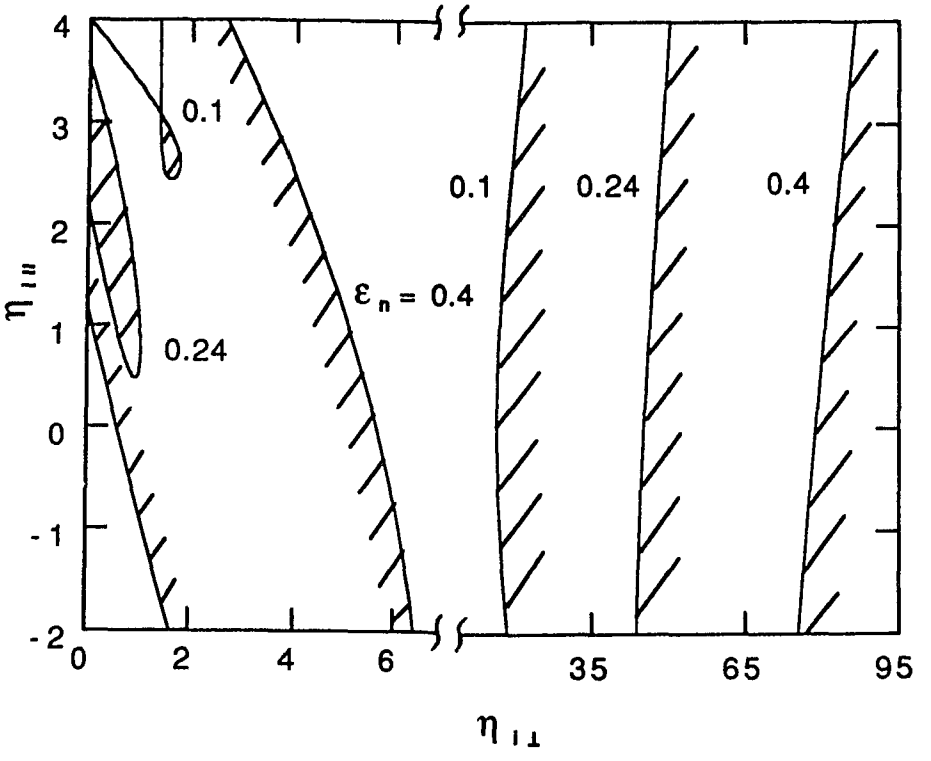

Fig. 5.6 The marginal stability diagram for large ε_n with both electron and ion collisions when $\tau_i = \tau_\perp = 1$, b=0.2 and $k_\parallel L_n = 0.1$. (a) $\varepsilon_n = 0.04$ and (b) $\varepsilon_n = 0.05$.

This stability region exists, even for large ε_n. The changes in the stability boundary with an increase in ε_n are also shown in Fig. 5.6. Due to the existence of this second stability regime, $\eta_{i\parallel}$ and $\eta_{i\perp}$ play completely different roles akin to the slab case. This can be understood in the following way. If we increase $\eta_{i\parallel}$ and keep $\eta_{i\perp}$ constant, the mode can always become unstable for large enough $\eta_{i\parallel}$. However, if we keep $\eta_{i\parallel}$ constant and increase $\eta_{i\perp}$, the mode can always enters the second stability regime at

large $\eta_{i\perp}$. In other words as the mode under discussion is basically a mixed slab and toroidal branch, at large enough $\eta_{i\parallel}$ and $\eta_{i\perp}$ slab branch contributions to the second stability regime appear. This second stability regime allows the possibility of stabilization of ITG modes in tokamaks *via* intense ICRF or neutral beam heating.

5.2. With trapped ions

The mixed slab and toroidal ITG mode was discussed with the dissipative trapped electrons. Now, a mixed slab and toroidal ITG mode is studied by including trapped ions that are always present in tokamaks. Specifically, the results of this study will be applied to an experiment in the Columbia Linear Machine (CLM).

The Columbia Linear Machine (SEN *et al.*, 1991) is a steady-state machine with a quiescent plasma column confined by a solenoidal magnetic field. A magnetic mirror cell is produced between a magnetic mirror coil and source coils. Electrons and ions can be trapped in the magnetic cell. By adjusting the mirror coil current, the magnetic curvature and trapped fraction can be varied to study the ITG instability under different experimental conditions. The slab branch of the ITG mode was identified in the CLM (SEN *et al.*, 1991). An experimental study of a transition between the slab and the toroidal ITG mode was also performed in the CLM (CHEN *et al.*, 1994). It was observed that the mode amplitude first increased and the mode frequency in the plasma frame decreased with an increase in the mirror ratio. However, with a further increase in the mirror ratio, the mode amplitude decreased as shown in Fig. 5.7.

Because the magnetic curvature created by the mirror coil is usually small, the magnetic drift resonance is not a dominant effect. On the other hand, because of the

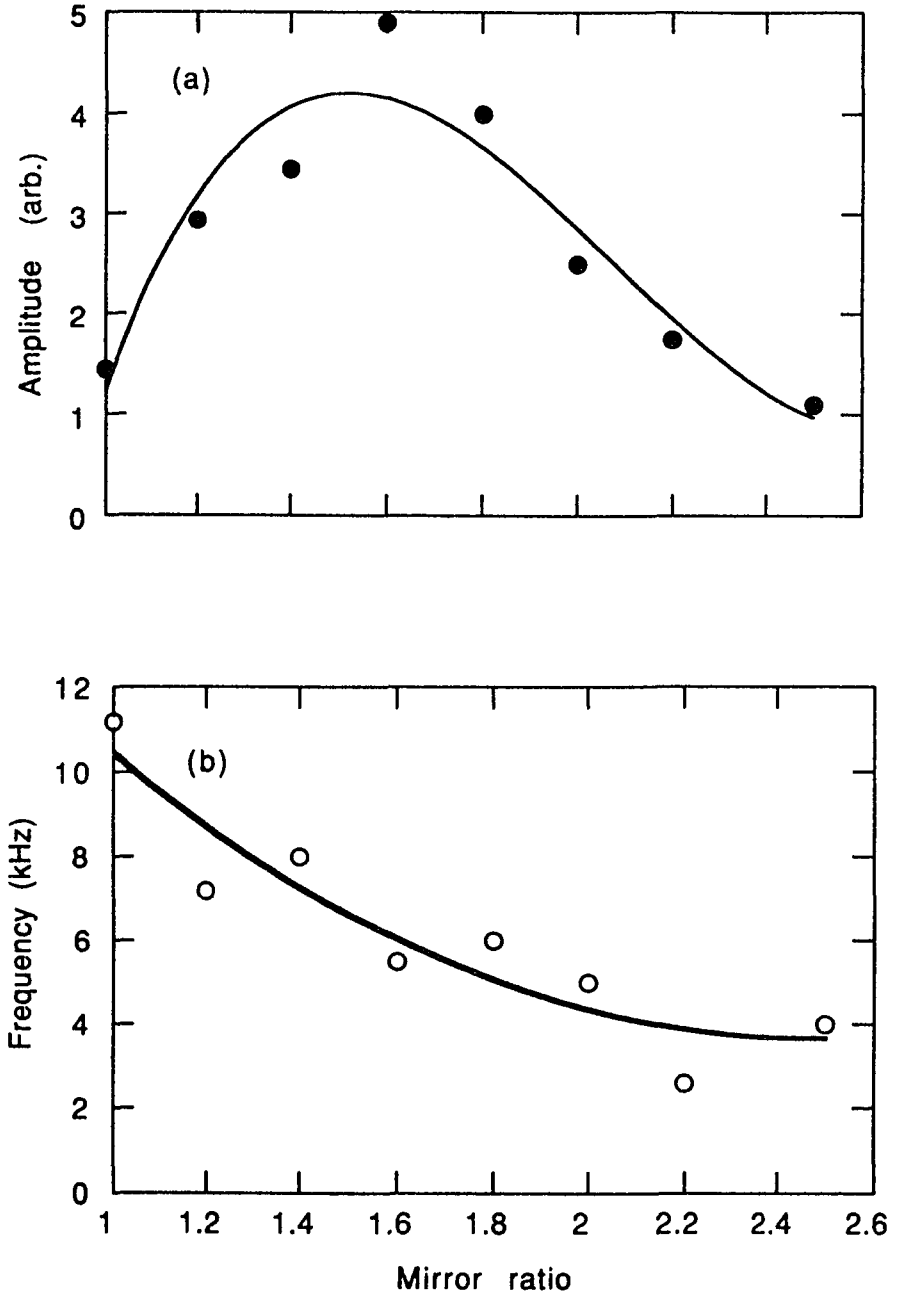

Fig. 5.7 Experimental results of the parametric dependence of the ITG mode on the mirror ratio: (a) mode amplitude, (b) real frequency.

finite parallel wavelength, the effect of the transit resonance becomes important. Therefore, an appropriate model for the CLM experiment should include the transit resonance for the transit ions and collisions as well as the first order correction of magnetic drifts for trapped ions and electrons. Because the ion bounce frequency is somewhat higher than the mode frequency, trapped ion response should be considered here. To simplify the problem, energy-independent Krook collision operators are used. By using the slab result, Eq. (3.1), for the transit ions and keeping the magnetic drift in Eq. (2.2) for the trapped ions, the following dispersion relation is obtained:

$$1+\tau_\perp+\left(1-\frac{n_t}{n_0}\right)S_0\left\{\tau_\parallel-\tau_\perp-\frac{\eta_{i\parallel}\omega_{*i}\omega}{k_\parallel^2}\right.$$

$$\left.+Z(\omega/k_\parallel)\left[\frac{\tau_\parallel\omega}{k_\parallel}-\frac{\omega_{*i}}{k_\parallel}\left(1+\frac{\eta_{i\parallel}\omega^2}{k_\parallel^2}-\frac{\eta_{i\parallel}}{2}-\eta_{i\perp}bG\right)\right]\right\}$$

$$-\frac{S_0 n_t}{n_0}\left\{\frac{1}{1+i\nu_{eff,i}/\omega}\left(\tau-\frac{\omega_{*i}}{\omega}(1-bG\eta_{i\parallel})\right)\right.$$

$$+\frac{\omega_{curv}}{2\omega(1+i\nu_{eff,i}/\omega)^2}\left(\tau_\perp-\frac{\omega_{*i}}{\omega}(1+\eta_{i\parallel}-\eta_{i\perp}bG)\right)$$

$$\left.+\frac{2\omega_{GB}}{\omega(1+i\nu_{eff,i}/\omega)^2}\left[(1-bG)\left(\tau_\perp-\frac{\omega_{*i}}{\omega}(1-\eta_{i\perp})\right)\right.\right.$$

$$+\frac{\eta_{i\parallel}\omega_{*i}}{\omega}(2-b-3bG+2b^2G)\Bigg]\Bigg\}$$

$$-\frac{n_t}{n_0}\left(\frac{\omega+\omega_{*i}}{\omega+i\nu_{eff,e}}-\frac{(\omega_{*i}(1+\eta_e)+\omega)(\tau_\parallel\omega_{curv}/2+2\tau_\perp\omega_{GB})}{(\omega+i\nu_{eff,e})^2}\right)=0\cdots(5.4)$$

where n_t/n_0 is the fraction of trapped particles and ω_{curv} and ω_{GB} is the magnetic curvature and grad-B drift frequencies, respectively. Here, $1+\tau_\perp$ is the adiabatic responses of electrons and ions.The second set of terms is the non-adiabatic response of transit ions, including the transit resonance. The magnetic drift for transit ions is neglected because the effect of the bad and good curvature seen by the transit ions in CLM cancels out. The third and fourth sets of terms are the trapped-ion and the trapped-electron responses, respectively.

This model is used to find the change in growth rate and real frequency with an increase in the mirror ratio. When the mirror current is increased, the trapped fraction and the magnetic curvature are increased simultaneously. In the experiment in the CLM, it was found that the parallel wavenumber decreased. Using the experimental parameters $\tau_\perp = 1$, $\tau_\parallel = 0.5$, $\eta_{i\parallel} = 1.5$, $\eta_{i\perp} = 3$, $L_n = 2$ (cm), b=0.044, $\nu_e/k_\parallel \sim 1$, $\nu_i/k_\parallel \sim 0.01$, and $k_\parallel = 0.1$- 0.02, the result is shown in Fig. 5.8. It basically agrees with the experimental observation (CHEN *et al.*, 1994) as shown in Fig. 5.7. The growth rate first increases because of the decrease in parallel wavenumber as well as the increasing extra drive from the increasing magnetic curvature. Then the growth rate decreases due to the decrease in the number of resonant ions as well as the increase in the number of trapped

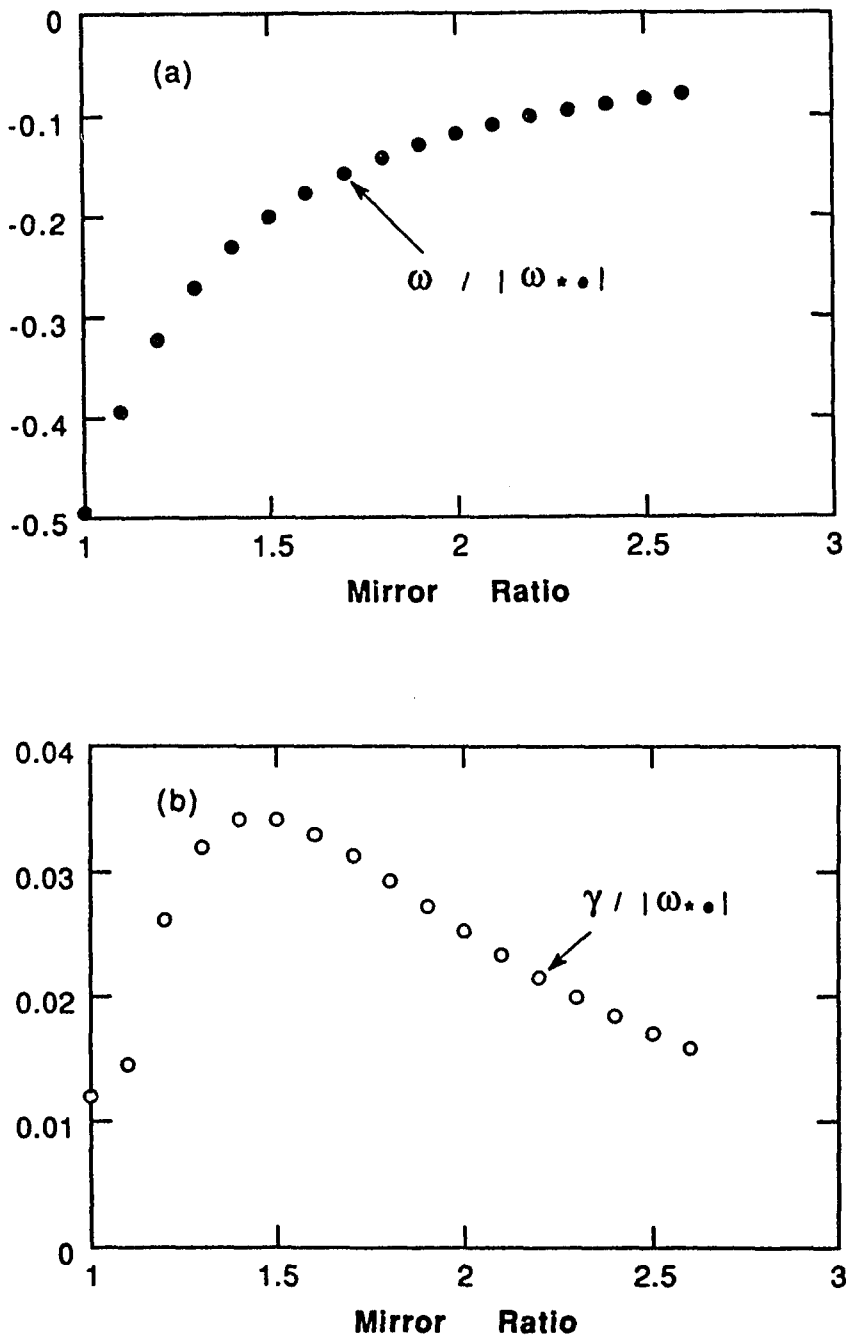

Fig. 5.8 Theoretical results based on Eq. (5.4) for CLM. (a) Growth rate and (b) real frequency as functions of the mirror ratio.

particles. The dissipative response of increasing number of the trapped electrons provides an increasing level of damping of this ion mode. The frequency decreases simply because of the decrease in the wavenumber, as the mode evolves toward a flute like curvature driven mode.

5.3. Conclusion

The mixed slab and toroidal ITG mode may be naturally expected in tokamaks. For this mode, a second stability regime is found at high $\eta_{i\perp}$. Unlike the slab case, the second stability regime forms a separate stability domain for the mixed mode because the coupling between the ion and electron branches in the slab limit causes a split of the stability region. The new stability domain has not been found in previous studies (KIM J.Y. *et al.*, 1992, ROMANELLI *et al.*, 1989) because either the effect of collisions was not considered or the anisotropic η_i was not taken into account. This new stability regime may provide a possible stabilization scheme for the ITG instability via intense ICRH or NBI heating. A model for an experiment on the mixed slab and toroidal ITG mode in the CLM is also proposed. This mixed slab and toroidal mode with trapped ions appears to predict the main features of the experimental results.

CHAPTER 6

NON-LOCAL EFFECT ON ITG MODE

In the previous chapters, the local analysis was used to investigate the ITG instabilities. The results obtained are only valid in a region where the gradients in plasma parameters do not vary too much. However, this assumption is not often good. In this chapter, a non-local analysis is used to find how the stability regime of the ITG mode changes when some non-local effects are considered.

The perturbation method is used to solve the non-local problem. In particular, the non-local effect is assumed to be a small perturbation to the local result and so the non-local correction can be obtained by an expansion. The advantage of using this method is that the physics of the non-local effect can be seen by comparing this result with the local result.

First, the non-local effect on the slab ITG mode is discussed. Then, the no-local effect on the mixed slab and toroidal ITG mode is investigated.

6.1. Non-local effect on slab ITG

6.1.1. Non-local η_i

In the local analysis, η_i is considered as a constant. However, it may not be true in reality. The plasma in the CLM is used as an example. Consider a cross section of the

plasma column in the CLM. Near the center and the edge, the temperature gradient is small. However, in the intermediate region, the temperature drops sharply and so the temperature gradient has a large value. If the density gradient is constant, η_i should also have a larger value in the intermediate region. A simple model for this is to assume that η_i changes quadratically with the radial position x:

$$\eta_{i\perp}(x) = \eta_{i\perp}\left(1 - \frac{(x-x_0)^2}{L_\perp^2}\right)$$

$$\eta_{i\parallel}(x) = \eta_{i\parallel}\left(1 - \frac{(x-x_0)^2}{L_\parallel^2}\right)$$

where x_0 is the position at which both $\eta_{i\parallel}(x)$ and $\eta_{i\perp}(x)$ reach their maximum value $\eta_{i\parallel}$ and $\eta_{i\perp}$, respectively.

For the non-local case, the amplitude of the perturbed electric potential is clearly not constant in x. The treatment of x-dependence can be done via $k_y^2 \rightarrow k_y^2 - d^2/dx^2$ in the local dispersion relation. By including the effects of the non-local temperature gradient and potential, the dispersion relation is now replaced by the following mode equation:

$$\left[1+\tau_\perp - \langle\cdots\rangle + \left(a_\parallel \eta_{i\parallel}\frac{\partial\langle\cdots\rangle}{\partial\eta_{i\parallel}} + a_\perp \eta_{i\perp}\frac{\partial\langle\cdots\rangle}{\partial\eta_{i\perp}}\right)\hat{x}^2 + \frac{\partial\langle\cdots\rangle}{\partial b}\frac{d^2}{d\hat{x}^2}\right]\phi = 0$$

where $\hat{x} = (x - x_0)/\rho_i$, $a_\parallel = (\rho_i/L_\parallel)^2$, $a_\perp = (\rho_i/L_\perp)^2$ and $\langle\cdots\rangle$ is the non-adiabatic ion response in Eq. (3.1). This is a Weber-type equation, yielding the eigenvalue condition:

$$1+\tau_\perp - \langle\cdots\rangle = (2l+1)\left[-\frac{\partial\langle\cdots\rangle}{\partial b}\left(a_\parallel \eta_{i\parallel}\frac{\partial\langle\cdots\rangle}{\partial\eta_{i\parallel}} + a_\perp \eta_{i\perp}\frac{\partial\langle\cdots\rangle}{\partial\eta_{i\perp}}\right)\right]^{1/2}$$

The marginal stability boundary with the non-local corrections can be obtained by solving this equation. The result is shown in Fig 6.1, where the parameters chosen

correspond to a typical CLM experiment. Only the result for the poloidal harmonic number m=2 is given because this is the only ITG mode observed in the experiment. Here, maximum $\eta_{i\parallel}(x)$ and $\eta_{i\perp}(x)$ at $x = x_0$ are compared with the local result. It is seen that the threshold values $\eta_{i\parallel}(x)$ and $\eta_{i\perp}(x)$ are higher with the non-local correction. The reason for this is that the non-local effect of the lower value of $\eta_{i\parallel}(x)$ and $\eta_{i\perp}(x)$ away from $x = x_0$ lowers the average $\eta_{i\parallel}$ seen by the wave.

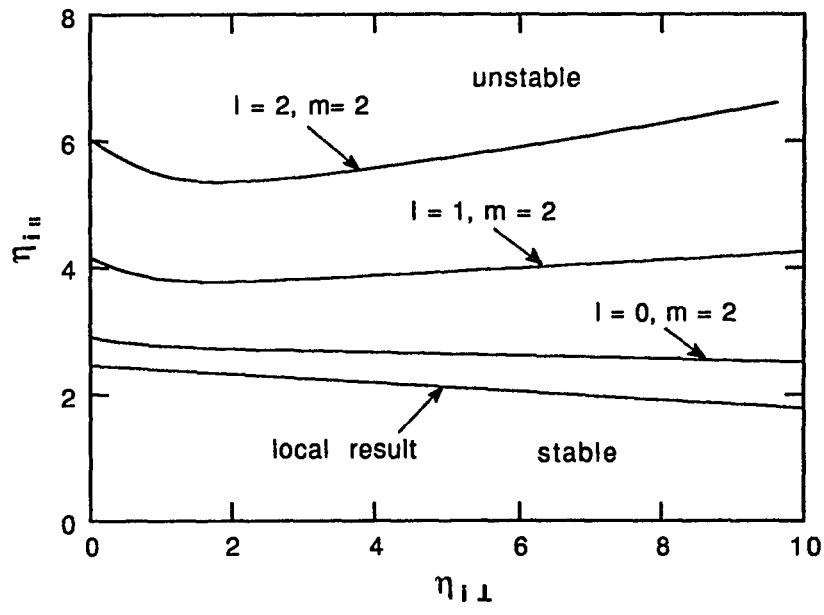

Fig. 6.1 The stability regimes with a non-local temperature gradient. Here, maximum $\eta_{i\parallel}(x)$ and $\eta_{i\perp}(x)$ at $x = x_0$ are compared with the local result.

6.1.2. Magnetic shear

The magnetic shear can be produced by the current flow in the plasma column. In the slab geometry, the magnetic field has the form $\mathbf{B} = B_0(\mathbf{e}_z + \mathbf{e}_y\, x/L_s)$ with L_s the shear scale length. Now, the magnetic field is also dependent of the position x.

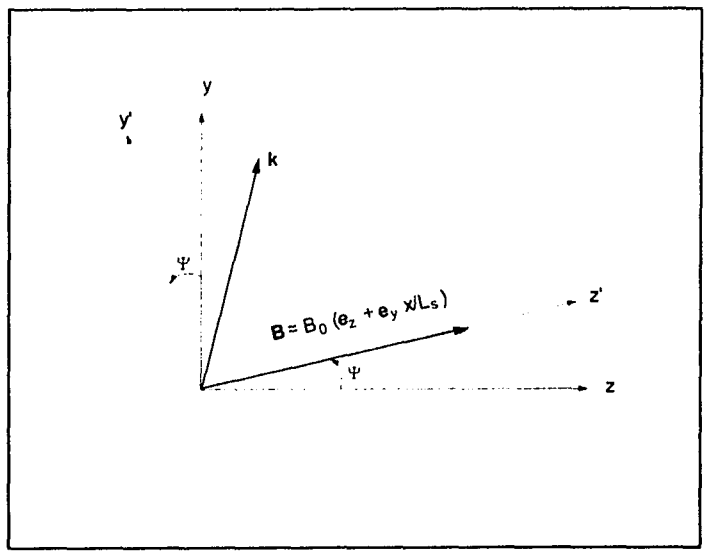

To study magnetic shear, a rotated coordinate system is introduced for the magnetic field at the position x. The coordinate system is rotated around the x-axis in such a way that the magnetic field is in the z-direction in the new coordinate system. The angle of the rotation is $\psi = \tan^{-1}(x/L_s)$. In the new coordinate system, the component of wave vector becomes

$$k_y' = -k_\parallel \sin\psi + k_y \cos\psi$$

$$k_\parallel' = k_\parallel \cos\psi + k_y \sin\psi$$

For $k_\parallel << k_y$ and small magnetic shear $x/L_s << 1$, the above equation becomes $k_\parallel' = k_\parallel + k_y x/L_s$ and $k_y' = k_y$. It is seen that the magnetic shear can be included by replacing the parallel wavenumber $k_\parallel$ by a magnetic shear dependent wavenumber $k_\parallel + k_y x/L_s$.

The mode equation with magnetic shear is given by

$$\left[1+\tau_\perp-\langle\cdots\rangle-\frac{\partial^2\langle\cdots\rangle}{\partial k_\parallel^2}\left(\frac{bs^2\hat{x}^2}{2}\right)\hat{x}^2+\frac{\partial\langle\cdots\rangle}{\partial b}\frac{d^2}{d\hat{x}^2}\right]\phi=0$$

with $s = L_n/L_s$. This is also a Weber equation, which yields the eigenvalue condition

$$1+\tau_\perp-\langle\cdots\rangle=(2l+1)\left[\frac{\partial\langle\cdots\rangle}{\partial b}\frac{\partial^2\langle\cdots\rangle}{\partial k_\parallel^2}\left(\frac{bs^2\hat{x}^2}{2}\right)\right]^{1/2}$$

For simplicity, the stability regime can be obtained by substituting the zeroth order results into the RHS of the above equation. The result for l = 0 is plotted in Fig. 6.2.

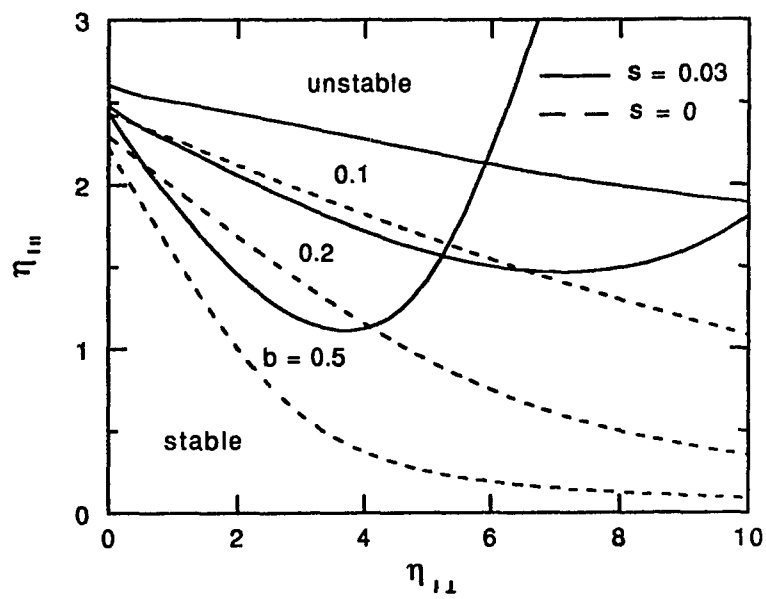

Fig. 6.2 The marginal stability boundaries with magnetic shear for $\tau_\parallel = \tau_\perp = 1$ and $k_\parallel L_n$=0.1.

Again, a marginal stability curve with a second stable regime is found as in the slab ITG mode with dissipative trapped electrons. We see that magnetic shear can also provide sufficient damping to produce a non-monotonic marginal stability boundary with second stable regimes.

6.2. Non-local effects on mixed slab and toroidal mode

In this part, the study of the mixed slab and toroidal ITG instability is extended to include such non-local effects as magnetic shear, non-local magnetic curvature and grad-B drifts. Instead of using (x, y, z), a new co-ordinate system (r, θ, ζ) is used to quantitatively describe these non-local effects. The geometry for an axisymmetric toroidal plasma is shown here, where r is the toroidal minor radius of a particular magnetic surface, θ is the poloidal angle and ζ is the toroidal angle, respectively. The relation between (x, y, z) and (r, θ, ζ) is given by $x = r - r_0$, $y = -r\theta$, and $z = R\xi$.

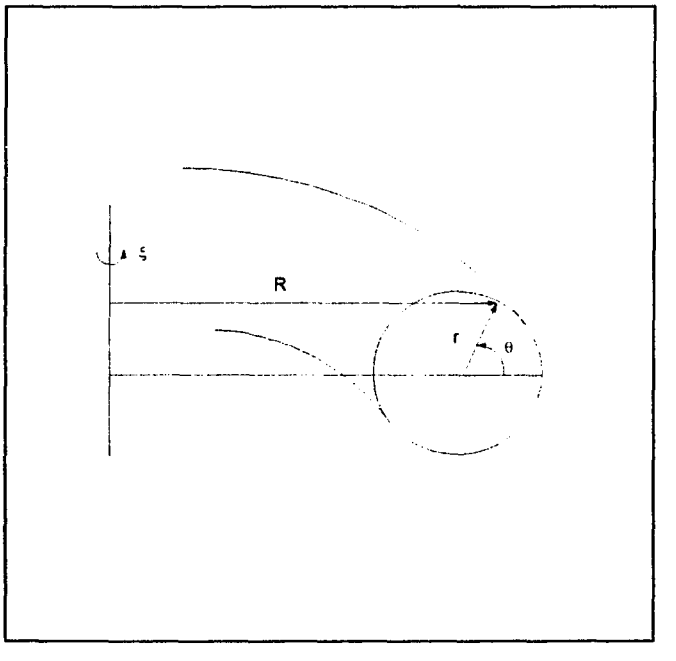

The plasma is confined by a toroidal magnetic field B_t. A poloidal magnetic field B_p is produced by a current within the plasma itself. The safety factor is defined by $q(r) = rB_t/RB_p$, which is used in the following discussion to describe some non-local tokamak properties.

6.2.1 Non-local Considerations

(1) Non-local potential

The perturbed electric potential has a form

$$\phi(r,\theta,\zeta,t)=\phi(r,\theta)\exp[i(n\zeta-m\theta-\omega t)] \quad \cdots(6.1)$$

where m is the poloidal mode number. The amplitude of the potential is periodic in θ, and contains the slow poloidal variation $|\partial \ln\phi/\partial\theta| << m$.

By following the same procedure as in the slab case, the perturbed ion density due to the non-local potential can be expressed as

$$\frac{n_i}{n_0}=\frac{e}{T_e}\left[-\tau_\perp+\langle\cdots\rangle-\frac{d\langle\cdots\rangle}{db}\frac{d^2}{d\hat{r}^2}\right]\phi(r,\theta,\zeta,t)$$

where $\hat{r} \equiv r/\rho_i$.

(2) Magnetic shear

As shown in the slab case, when magnetic shear is included, parallel wave number is no longer constant. Therefore, perturbed ion density has an extra contribution from the non-local parallel wave number.

The discussion for magnetic shear for tokamaks is similar to the slab case. The parallel wave number due to magnetic shear can also be written as $k_\parallel = k_{\parallel 0} + k_\theta(r-r_0)/L_s$. The only difference is that the magnetic shear parameter for tokamak is now $\hat{s}$

$\equiv$ r q'/q. Using $L_s \equiv [(\varepsilon/q^2)(dq/dr)]^{-1}$ with $\varepsilon \equiv r/R$, the shear parameter $s=L_n/L_s$ in the slab case is replaced by $s \rightarrow \varepsilon_n \hat{s}/q$. Therefore, the change in the perturbed ion density due to magnetic shear becomes

$$\frac{n_i}{n_0} = \frac{e}{T_e}\left[-\tau_\perp + \langle\cdots\rangle + \frac{\partial^2\langle\cdots\rangle}{\partial k_\parallel^2}\left(\frac{b\epsilon_n^2\hat{s}^2(\hat{r}-\hat{r}_0)^2}{2q^2}\right)\right]\tilde{\phi}(r,\theta,\zeta,t)\,.$$

(3) Magnetic curvature and grad-B drifts

By using $\mathbf{v}_D \propto \mathbf{B}\times\nabla B$ with $B = B_0[1-(\varepsilon/R)\cos\theta]$, it can be shown that the magnetic (curvature and grad-B) drift velocity $\mathbf{v}_D$ is in the direction of $\mathbf{n} = -\cos\theta\,\mathbf{e}_\theta - \sin\theta\,\mathbf{e}_r$, where $\mathbf{e}_\theta$ and $\mathbf{e}_r$ are unit vectors in the poloidal and radial directions. Then, the non-local drift frequency $\omega_D(r,\theta) = \mathbf{k}\cdot\mathbf{v}_D$ can be written as

$$\omega_D(r,\theta) = \omega_D\left(\cos\theta + \frac{ir}{m}\sin\theta\frac{\partial}{\partial r}\right)$$

where $k_\theta = -m/r$ and $k_r = -i\,\partial/\partial r$ are used to obtain the above equation. For small θ, the above drift frequency reduces to

$$\omega_D(r,\theta) \approx \omega_D\left(1-\frac{\theta^2}{2}+\frac{ir\theta}{m}\frac{\partial}{\partial r}\right)$$

Since the non-local part of the drift frequency is considered as a small parameter, the perturbation method is used to obtain the perturbed ion density by keeping only the lowest order correction from the non-local drift frequency:

$$\frac{n_i}{n_0}=\frac{e}{T_e}\left[-\tau_\perp+\langle\cdots\rangle-\omega_D\left(\frac{\theta^2}{2}-i\frac{\theta}{\sqrt{b}}\frac{\partial}{\partial\hat{r}}\right)\frac{\partial\langle\cdots\rangle}{\partial\omega_D}\right]\phi(r,\theta,\zeta,t) \quad \cdots(6.2)$$

The new feature in the above expression is that besides the radial position r, a new dimension of θ appears from the non-local magnetic drift. Unlike the non-local slab case where only an one-dimensional (1D) eigenmode equation is relevant, now the mode equation is a two-dimensional (2D) differential equation. Usually, it is a formidable task to obtain a general solution to the 2D eigenmode equation. In the following section, an approximation is introduced to deal with this problem.

6.2.2 Stability regime with non-local corrections

(1) Large-n approximation

The large-n approximation is used to convert a 2D eigenmode equation into an 1D equation.

The poloidal mode number m can be written as

$$m=nq(r_0)\approx nq(r)-n\frac{dq}{dr}(r-r_0)\,.$$

Now define $S(r)\equiv (r-r_0)/\Delta r_s$ with $\Delta r_s\equiv (nq')^{-1}$ being the separation of mode rational surfaces for a given n. In terms of S(r), the non-local potential given by Eq. (6.1) can be expressed as

$$\phi(r,\theta,\zeta,t) = [\phi(S,\theta)\exp(iS\theta)]\exp\{in[\zeta - q(r)\theta] - i\omega t\} \quad \cdots(6.3)$$

In the above equation, [φ⟨S,θ⟩exp⟨iSθ⟩] gives the variation of the electric potential along the magnetic field lines because [ζ - q(r)θ] is approximately constant along the field lines. In particular, this variation of the potential along the field lines is

$$\frac{\partial}{\partial l_{\parallel}}\phi = \phi\left[\frac{1}{qR}\left(\frac{\partial}{\partial\theta}\ln\phi(S,\theta) + iS\right)\right].$$

The variation along a radial direction can also be obtained by using Eq. (6.2):

$$\frac{\partial}{\partial r}\phi = \phi\left\{\frac{\partial}{\partial r}\ln[\phi(S,\theta)\exp(iS\theta)] - i\theta nq'\right\}.$$

The large-n approximation assumes that n >> (∂ln[φ(S,θ)exp(iSθ)]/∂r)/q' ~ 1 in the above equation. Then, the variation of potential is solely determined by the phase term -i nq(r)θ. With this approximation, the poloidal angle θ can be replaced by i (1/nq') (∂/∂r) = i ∂/∂S. Thus, the two-dimensional equation (6.2) becomes only dependent on r.

(2) Eigenmode equation

The eigenmode equation can be obtained from the quasi-neutrality condition $n_i = n_e$. The perturbed electron density has the same form as in the local case. The non-local effects discussed in Sec. 6.2.1 are included in the expression of the perturbed ion density with the large-n approximation. The eigenmode equation is then given by

$$\left\{1 + \tau_{\perp} - i\delta - \langle\cdots\rangle - \frac{\partial^2\langle\cdots\rangle}{\partial k_{\parallel}^2}\frac{\epsilon_n^2 S^2}{2q^2} + \left[b\hat{s}^2\frac{\partial\langle\cdots\rangle}{\partial b} - \omega_{GB}\left(\frac{1}{2} - \hat{s}\right)\frac{\partial\langle\cdots\rangle}{\partial\omega_{GB}}\right]\frac{d^2}{dS^2}\right\}\phi(S) = 0$$

Note that this is only an 1D equation. Here, $\hat{r}$-$\hat{r}_0$ = S/($b^{1/2}\hat{s}$) is used to replace $\hat{r}$ with S. The fourth, fifth and sixth terms in the LHS are the non-local contributions from the magnetic shear, electric potential and magnetic drift respectively.

The above eigenmode equation is also a Weber-type equation. The eigenvalue can be solved as

$$1+\tau_\perp - i\delta - \langle\cdots\rangle = (2l+1)\left\{\frac{\partial^2\langle\cdots\rangle}{\partial k_1^2}\frac{\epsilon_n^2}{2q^2}\left[b\hat{s}^2\frac{\partial\langle\cdots\rangle}{\partial b} - \omega_{GB}\left(\frac{1}{2}-\hat{s}\right)\frac{\partial\langle\cdots\rangle}{\partial\omega_{GB}}\right]\right\}^{1/2} \quad \cdots(6.4)$$

where l is the radial harmonic number. The non-local corrections appear in the RHS of the equation. When the RHS of the equation vanishes, the above eigenvalue condition is simply the local dispersion relation given by Eq. (5.1). This eigenvalue condition contains all the information about the new stability regime with the non-local corrections.

(3) Marginal stability boundaries

With the CER and small b approximation, a simple analytic form of the dispersion relations can be derived. This method can provide basic features to the marginal stability boundary and can also be used as a way to confirm the numerical calculations. The numerical calculation without any approximation is the other way to obtain the stability regime. This method gives more accurate results although there are many technical problems. For the non-local study, the latter approach is used to obtain the stability regime. A computer code is developed to solve Eq. (6.4).

The main purpose is to examine how the marginal stability boundaries vary by

including the non-local effects discussed in section 6.2.1. The electron and ion collisions are retained because it was shown that the second stability regime is affected by collisions. Two figures are given here to show the effect of non-local correction.

Figure 6.3 is used to compare with the local result given by Fig. 5.5. It is found that the stability regime for the ion branch is expanded with non-local contribution while the stability regime for the electron branch is shrunk dramatically. The non-local effect is so strong that the coupling of the upper and lower branches no longer exists. The different effects for the ion and electron branch can be understood by noticing the similarity between this case and that of the local analysis when the dissipative trapped electrons were included. The non-local contribution can also be considered as reduction of the growth rate of the ion branch. However, when the wave propagates in the electron diamagnetic direction, the non-local correction changes the role and becomes an increase in the growth rate.

Figure 6.4 shows how the stability regime varies with increasing ε_n. Although the second stability regime is not separated as in the local case, it is still there for the ion branch. If $\eta_{i\perp}$ is increased for positive $\eta_{i\parallel}$, the wave can become stable due to the existence of the second stability regime.

6.3. Conclusion

For the mixed slab and toroidal mode, a second stability regime still exists at high $\eta_{i\perp}$ for the ion branch. However, it is not separated from the stability regime at low $\eta_{i\perp}$. The non-local effects have a stabilizing effect on the ion branch but a destabilizing effect on the electron branch. This correction is so significant that it overcomes the effect of coupling between ion and electron branches.

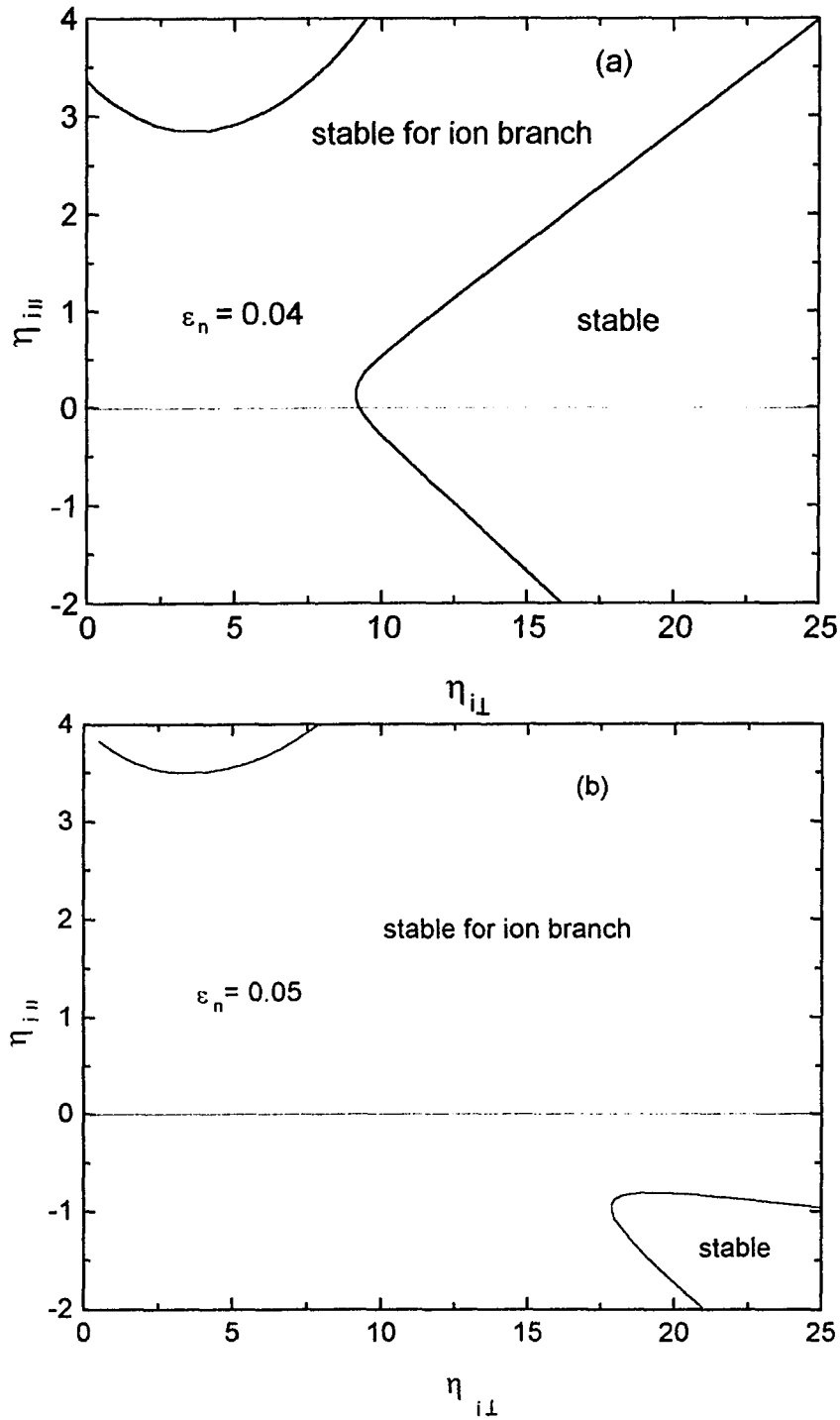

Fig. 6.3 The stability regime with non-local effects. It is used to compare with the local result given by Fig. 5.5.

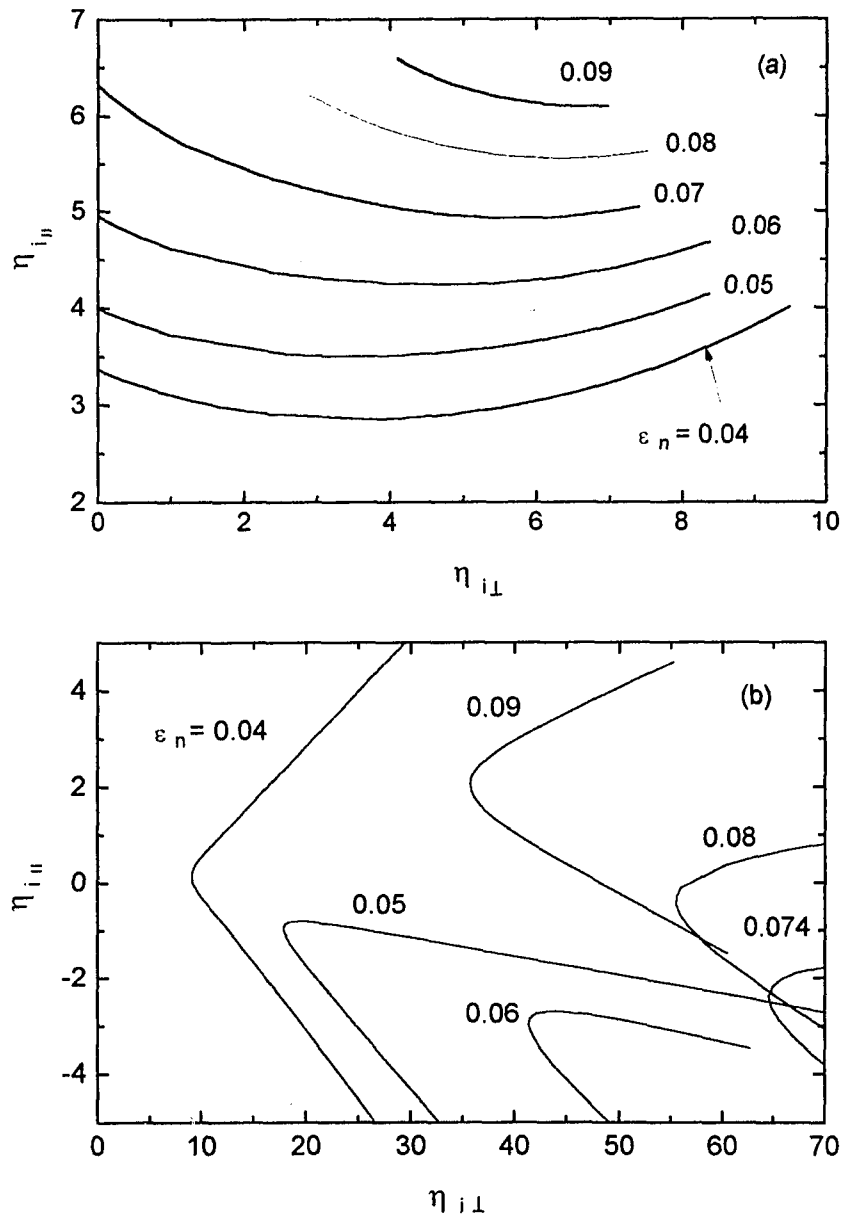

Fig. 6.4 The stability regime with non-local effects (a) the ion branch and (b) the electron branch.

CHAPTER 7

SUMMARY

In this thesis, the effect of anisotropic temperature gradient and collisions on the ITG instabilities has been investigated. The slab ITG instability is associated with the transit resonance. A simple analytical expression for the stability regime was first obtained in the collisionless case. The results show that $\eta_{i\parallel}$ is always needed to trigger the instability. However, $\eta_{i\perp}$ only affects the mode through the FLR effect because the variation of gyroradius leads to energy exchange between the resonant ions and the wave. There are two branches of stability boundaries. The upper and lower boundaries correspond to the wave propagating in the ion and electron diamagnetic drift directions, respectively. Increasing $\eta_{i\parallel}$ and $\eta_{i\perp}$ destabilizes the ion branch but stabilizes the electron branch. Then, when the dissipative trapped electrons are included, the stability regime can be modified significantly, especially for weak transit resonance. A second stability regime is found at large $\eta_{i\perp}$ for the ion branch while the electron branch becomes more unstable at small $\eta_{i\perp}$. This occurs because the negative energy wave becomes the positive energy wave. Thus, collisions from the dissipative trapped electrons change its role to stabilize the ion branch and destabilize the electron branch. Finally, it was found that ion collisions only weakly affect the mode.

The toroidal ITG mode is related to the magnetic drift resonance. In the

collisionless limit, both $\eta_{i\parallel}/\varepsilon_n$ and $\eta_{i\perp}/\varepsilon_n$ can drive the instability. The reason for this is that the magnetic drift resonance depends on both parallel and perpendicular velocity. The instability can occur for either ion or electron branches. However, the nature of the instability is totally different. For the ion branch, which is expected at large ε_n, the mode is driven unstable by the power transferred from the resonant ions to the wave. However, for the electron branch, there is no the magnetic drift resonance. This mode is destabilized by the interchange effect from bad magnetic curvature. The effect of collisions was also studied. Similar to the slab case, the dissipative trapped electrons can stabilize the ion branch but destabilize the electron branch. Ion collisions only weakly affect the mode. The other type of the toroidal ITG mode was considered with trapped ions. For the TFTR experiment with the nearly flat density profile, only the resonant ion branch of this mode is important. The perpendicular temperature gradient is crucial to drive the instability. The threshold value of the temperature gradient is increased by a factor of $1/\varepsilon^{1/2}$ since only the trapped ions participate in the resonance. This threshold can be further enlarged by both electron and ion collisions.

The study of the mixed slab and toroidal ITG mode deals with the situation where both magnetic and drift resonances are included. This mode may be naturally expected in tokamaks. The CER approximation can be used to get an analytical form of the dispersion relation. This result is compared with the numerical solution of the dispersion relation without any approximation. These two results agree well. For the collisionless case, a coupling between the ion and electron branches was found due to the toroidal contribution. The coupling causes the stability regime to break into two separated regions in the $\eta_{i\parallel}$-$\eta_{i\perp}$ plane. With collisions, the dissipative trapped electrons can significantly reduce the first stability regime at small $\eta_{i\perp}$ but expand the second

stability regimes at large $\eta_{i\perp}$. The mixed slab and toroidal mode with trapped ions was also considered as a model for the experiment in the CLM. Both frequency and growth rate were calculated and agree well with the experimental result.

The non-local effect on the ITG stability was also studied. For the slab case, the non-local η_i and magnetic shear have stabilizing effect on the mode. For the mixed slab and toroidal mode, the non-local effects of magnetic shear and pitch angle dependence of the magnetic drift resonance were included in the model. The numerical solution for the mode equation was obtained. Compared with the local result, the ion branch becomes more stable while the electron branch becomes more unstable. This effect can overcome the effect of coupling between the ion and electron branches. Consequently, the second stability regime is not separated from the first one.

One of the most interesting results of this research is that a second stability regime for the ion branch was found at large $\eta_{i\perp}$ with the dissipative trapped electrons. This new stability regime may provide a possible stabilization scheme for the ITG instability via intense ICRH or NBI heating.

APPENDIX

DERIVATION OF THE DISPERSION RELATION WITH THE CER APPROXIMATION

With CER approximation $u/2 + 2\tau_\perp p^2/\tau_\parallel \rightarrow 4(u/2+2p^2)/3$, the perturbed ion density of Eq. (2.2) reduces to

$$\frac{n_i}{n_0} = \frac{e\phi}{T_e}\left(-\tau_\perp + \left\langle \frac{\tau_\perp \omega + (\tau_\parallel - \tau_\perp) k_\parallel p - \omega_{*i}\left(1 - \eta_{i\perp} - \eta_{i\parallel}/2 + p^2\eta_{i\parallel} + \eta_{i\perp}u/2\right)}{\omega + i\nu_i - k_\parallel p - \omega_D(u/2+p^2)} \right\rangle\right).$$

This result can be rewritten as

$$\langle 1\rangle(\tau_\perp - \tau_\parallel)$$

$$+\left[\tau_\parallel \frac{\omega}{k_\parallel} - i\frac{\nu_i}{k_\parallel}(\tau_\perp - \tau_\parallel) - \frac{\omega_{*i}}{k_\parallel}\left(1 - \eta_{i\perp} - \frac{\eta_{i\parallel}}{2}\right)\right]\left\langle \frac{k_\parallel}{\omega + i\nu_i - k_\parallel p - 4\omega_D(u/2+p^2)/3} \right\rangle$$

$$-\left(\frac{4\omega_D}{3k_\parallel}(\tau_\perp - \tau_\parallel) - \frac{\omega_{*i}\eta_{i\perp}}{k_\parallel}\right)\left\langle \frac{k_\parallel u/2}{\omega + i\nu_i - k_\parallel p - 4\omega_D(u/2+p^2)/3} \right\rangle$$

$$-\left(\frac{4\omega_D}{3k_\parallel}(\tau_\perp-\tau_\parallel)-\frac{\omega_{*i}\eta_{i\parallel}}{k_\parallel}\right)\left\langle\frac{k_\mu p^2}{\omega+iv_i-k_\mu p-4\omega_D(u/2+p^2)/3}\right\rangle$$

By expanding $J_0^2((bu)^{1/2}) \approx 1\text{-}bu/2$ and changing integration vairibles $u\rightarrow 2v^2\sin^2\theta$, $p\rightarrow v\cos\theta - 3k_\parallel/8\omega_D$,

$$\left\langle\frac{k_\parallel}{\omega+iv_i-k_\mu p-4\omega_D(u/2+p^2)/3}\right\rangle$$

$$=\frac{2k_\parallel}{\sqrt{\pi}}\int_0^{+\infty}dv\ v^2\int_0^{\pi}d\theta\ \sin\theta(1-bv^2\sin^2\theta)$$

$$\times\frac{\exp(-v^2+3k_\parallel v\cos\theta/4\omega_D-9k_\parallel^2/64\omega_D^2)}{\omega+iv_i-4\omega_D v^2/3-3k_\parallel^2/16\omega_D}.$$

Let

$$F_0(\alpha,\beta)$$

$$\equiv\frac{2k_\parallel}{\sqrt{\pi}}\int_0^{+\infty}dvv^2\int_0^{\pi}d\theta\ \sin\theta\frac{\exp(-\beta v^2+3\alpha k_\parallel v\cos\theta/4\omega_D-9k_\parallel^2/64\omega_D^2)}{\omega+iv_i-4\omega_D v^2/3-3k_\parallel^2/16\omega_D}$$

and

$$F(\alpha,\beta) \equiv F_0(\alpha,\beta) + b\left[\frac{\partial F_0}{\partial \beta} + \left(\frac{4\omega_D}{3k_\parallel}\right)^2 \frac{\partial^2 F_0}{\partial \alpha^2}\right].$$

It is easy to prove that

$$\langle 1 \rangle = 1 - b,$$

$$\left\langle \frac{k_\parallel}{\omega + i\nu_i - k_\parallel p - 4\omega_D(u/2+p^2)/3} \right\rangle = F\big|_{\alpha,\beta=1}$$

$$\left\langle \frac{k_\parallel p^2}{\omega + i\nu_i - k_\parallel p - 4\omega_D(u/2+p^2)/3} \right\rangle = -\left(\frac{\partial F}{\partial \alpha} - \frac{16\omega_D^2}{9k_\parallel^2}\frac{\partial^2 F}{\partial \alpha^2} - \frac{9k_\parallel^2 F}{64\omega_D^2}\right)\Bigg|_{\alpha,\beta=1}$$

$$\left\langle \frac{k_\parallel u/2}{\omega + i\nu_i - k_\parallel p - 4\omega_D(u/2+p^2)/3} \right\rangle = -\left(\frac{\partial F}{\partial \beta} + \frac{16\omega_D^2}{9k_\parallel^2}\frac{\partial^2 F}{\partial \alpha^2}\right)\Bigg|_{\alpha,\beta=1}$$

In the above formalism, F_0 is the only function which remains undetermined. Upon integrating over θ, F_0 becomes

$$F_0(\alpha,\beta) = \frac{8\omega_D \exp\left[-9k_\parallel^2(1-\alpha^2/\beta)/64\omega_D^2\right]}{3\alpha\sqrt{\pi}}$$

$$\times \int_0^{+\infty} dv\, v\, \frac{\exp\left[-\beta(v+3\alpha k_\parallel/8\beta\omega_D)^2\right] - \exp\left[-\beta(v-3\alpha k_\parallel/8\beta\omega_D)^2\right]}{\omega + i\nu_i - 4\omega_D v^2/3 - 3k_\parallel^2/16\omega_D}$$

$$= \frac{1}{\alpha}\left[Z\left(-\sqrt{\frac{3\beta(\omega + i\nu_i)}{4\omega_D} + \frac{9\beta k_l^2}{64\omega_D^2}} + \frac{3\alpha k_l}{8\sqrt{\beta}\omega_D} \right) \right.$$

$$\left. - Z\left(-\sqrt{\frac{3\beta(\omega + i\nu_i)}{4\omega_D} + \frac{9\beta k_l^2}{64\omega_D^2}} - \frac{3\alpha k_l}{8\sqrt{\beta}\omega_D} \right) \right]$$

$$\times \exp\left[-9k_l^2 (1 - \alpha^2/\beta) / 64\omega_D^2 \right] .$$

REFERENCES

ANTONSEN T., COPPI B., and ENGLADE R. (1979) *Nucl. Fusion* **19**, 641.

BIGLARI H., DIAMOND P.H. and TERRY P.W., (1988) *Phys. Fluids* **31**, 2644.

BIGLARI H., DIAMOND P.H., and ROSENBLUTH M.N. (1989) *Phys. Fluids* **B1**, 109.

BHATNAGAR P.L., GROSS E.P. and KROOK M. (1954) *Phys. Rev.* **94**, 511.

CHEN J. and SEN A.K. (1994) To be published in *Phys Rev.Lett.* , July.

COPPI B., ROSENBLUTH M.N.and SAGDEEV R.Z. (1967) *Phys. Fluids* **10,** 582.

COPPI B. and PEGORARO F. (1977) *Nucl. Fusion* **17**, 5.

CREAVES R.G., et al., (1991) *Experiment Study of the Effects of Magnetic Curvature and Trapped Particles on an Ion-Temperature-Gradient Driven Instability*, Plasma Laboratory Report, Columbia University, New York.

DOMINGUEZ R.R. and WALTZ R.E. (1988) *Phys. Fluids* **31**, 3147.

DONG J.Q., HORTON W., and KIM J.Y. (1992) *Phys. Fluids* **B4**, 1867.

GAUTSCHI W. and CAHILL W.F., (1964) *Handbook of Mathematical Functions* (ABRAMOWITZ. M., Ed.), p. 227, U.S. Goverment Printing Office, Washington, D.C..

GREENWARD M.J. et al., (1984) *Phys Rev. Lett* **53**, 352.

GUZDAR P.N., CHEN L., TANG W.M., RUTHERFORD P.H. (1983) *Phys. Fluids* **26**, 673.

HASEGAWA A. (1975) *Plasma Instabilities and Nonlinear Effects* (Springer-Verlag, New York) pp. 18.

HORTON W., CHOI O.I., TANG W.M. (1981) *Phys. Fluids* **24** 1077.

HORTON W., ESTES W., BISKAMP R.D. (1980) *Plasma Phys.* **22**, 43.

JET Team, (1989) *Plasma Physics and Controlled Nuclear Fusion Research* 1988, Nice, (IAEA, Vienna), **Vol**. 1, p.215.

KADOMTSEV B.B., POGUTSE O.P. (1970) *Review of Plasma Physics* (LEONTOVICH M.A. Ed.) **Vol**. 5. Consultants Bureau, New York 249.

KADOMTSEV B.B., POGUTSE O.P. (1971) *Nucl. Fusion* **11**, 67.

KAUFMANN M. et al. (1989) *Plasma Physics and Controlled Nuclear Fusion Research* 1988, Nice, (IAEA, Vienna), **Vol**. 1, p. 229.

KAYE S.M. (1985) *Phys. Fluids* **28**, 2327.

KIM J.Y., HORTON W., and DONG J.Q. (1993) *Phys. Fluids* **B5**, 4030.

KIM J.Y., and HORTON W. (1991) *Phys Fluids* **B3**, 1167.

LEE G.S. and DIAMOND P.H. (1986) *Phys. Fluids* **29**, 3291.

MARCHAND R., TANG W.M. and REWOLDT G. (1980) *Phys. Fluids* **23**, 1164.

MATHEY O. and SEN A. K. (1989) *Phys. Rev. Lett.*, **62**, 268 .

MIGLIUOLO S. (1985) *Phys. Fluids* **28**, 2778.

MIKHAILOVSKII A.B. (1974) *Theory of Plasma Instabilities* (Consultants Bureau, New York) **Vol. 2**, pp. 55-58.

MIYAMOTO K., (1980) *Plasma Physics for Nuclear Fusion* (MIT Press, Cambridge, MA)

NAGAMI M., KASAI M., KITSUNEZAKI A., et al. (1984) *Nucl. Fusion* **24**, 183.

REWOLDT G. (1994) private communication.

ROMANELLI F. (1989) *Phys. Fluids* **B1**, 1018.

ROMANELLI F. and BRIGUGLIO S. (1990) *Phys. Fluids* **B2**, 754.

ROSENBLUTH M.N., ROSS D.W. and KOSTOMAROV D.P. (1972) *Nucl. Fusion* **12**, 3.

RUDAKOV R.I., SAGDEEV R.Z. (1961) *Sov. Phys. Dokl.* **6**, 415.

SCHISSEL D. P. et al., (1989) *Phys. Fluids* **B1**, 1843.

SEN A.K., CHEN. J and MAUEL M., (1991) *Phys Rev.Lett.* **66**, 429.

SOLDNER F., et al., (1988) *Phys. Rev. Lett.* **61**, 1055.

SUZUKI N., AIKAWA A. et al., (1989)*Plasma Physics and Controlled Nuclear Fusion Research* 1988, Nice, (IAEA, Vienna), **Vol**. 1, p. 207.

TAGGER M., LAVAL G. and PELLAT R. (1977) *Nucl. Fusion* **17**, 109.

TANG W. M., ADAM J. C. and ROSS D. W. (1977) *Phys. Fluids* **20,** 430.

TANG W.M., REWOLDT G., CHEN L. (1986) *Phys. Fluids* **29**, 3715.

TAYLOR J.B. and HASTIE R.J. (1968) *Plasma Physics* (Pergamon Press) **Vol. 10**, pp 479.

TERRY P., ANDERSON W., HORTON W. (1982) *Nucl. Fusion* **22**, 487.

WAGNER F., BECKER G., BEHRINGER K., CAMPBELL D. (1982) *Phys. Rev. Lett.* **49**, 1408.

WALTZ R.E., PFEIFFER W., DOMINGUEZ R.R. (1980) *Nucl. Fusion* **20**, 43.

WATARI et al., (1990) *Nucl. Fusion* **30**, 1197.

WATTERSON R.L., SLUSHER R.E. and SURKO C.M. (1985) *Phys. Fluids* **28**, 2857.

XU X.Q., ROSENBLUTH, M.N. (1991) *Phys. Fluids* **B 3**, 627.

XU X.Q., ROSENBLUTH, M.N., (1991) *Phys. Fluids* **B 3** 1807.

ZARNSTORFF M.C., GOLDSTON R.J., BELL M.G., BUSH C., FONCK R. J. et al., (1989) *Controlled Fusion and Plasma Physics* (Proc. 16th Eur. Conf., Venice, **13 B**, Part I, European Physical Society).

ZARNSTORFF M. C., BARNES C. W., EFTHIMION, P. C., HAMMETT G.W. et al., (1991) *Plasma Physics and Controlled Nuclear Fusion Research* (Proc. 13th Int. Conf. Washington, DC., 1990), **Vol. 2**, 109, IAEA, Vienna.